Electronic Supplementary Information

Hollow Capsules of Doped Carbon Incorporating Metal@Metal Sulfide and Metal@Metal Oxide Core–Shell Nanoparticles Derived from Metal-Organic Framework Composites for Efficient Oxygen Electrocatalysis

Feng Guo,[ab] Hui Yang,*[b] Lingmei. Liu,[c] Yu Han,[c] Abdullah M. Al-Enizi,[d] Ayman Nafady,[de] Paul E. Kruger,[f]

Shane G. Telfer,*[g] and Shengqian Ma*[b]

[a]Chongqing Key Laboratory of Inorganic Special Functional Materials, Yangtze Normal University, 16 Juxian Rd, Fuling, ChongQing, 408100 China.

[b]Department of Chemistry, University of South Florida 4202 E. Fowler Avenue, Tampa, Florida 33620, United States.

E-mail: huiy@mail.usf.edu; sqma@usf.edu

[c]Advanced Membranes and Porous Materials Center, Physical Sciences and Engineering Division, King Abdullah University of Science and Technology, Thuwal 23955–6900, Saudi Arabia

[d]Abdullah M. Al-Enizi,c Ayman Nafady, Chemistry Department, College of Science, King Saud University, Riyadh, 11451, Saudi Arabia.

[e]Chemistry Department, Faculty of Science, Sohag, 82524, Egypt.

[f]MacDiarmid Institute for Advanced Materials and Nanotechnology, Department of Chemistry, University of Canterbury, Christchurch 8140, New Zealand

[g]MacDiarmid Institute for Advanced Materials and Nanotechnology, Institute of Fundamental Sciences, Massey University, Palmerston North 4442, New Zealand
E–mail: s.telfer@massey.ac.nz

1. Chemicals

Zinc nitrate hexahydrate ($Zn(NO_3)_2 \cdot 6H_2O$, Sigma−Aldrich, >98%), cobalt(II) nitrate hexahydrate ($Co(NO_3)_2 \cdot 6H_2O$, Sigma−Aldrich, ≥98%), Nickel(II) nitrate hexahydrate ($Ni(NO_3)_2 \cdot 6H_2O$, Sigma−Aldrich, ≥98.5%), potassium hydroxide (KOH, Sigma−Aldrich, 90%), platinum on carbon (Pt/C, Sigma−Aldrich, 20wt.% Pt basis), Ruthenium(IV) oxide (RuO_2, Sigma−Aldrich, 99.9% trace metals basis), 2−methylimidazole (Sigma−Aldrich, 99%), tannic acid (TA, Sigma−Aldrich, ACS reagent), Nafion solution (5%, Alfa−Aesar), Benzene (Sigma−Aldrich, ≥99.9%), Ethanol (EtOH, Sigma−Aldrich, ≥99.8%) and Methanol (MeOH, Sigma−Aldrich, >99.8%) were obtained from commercial sources and used without further purification.

2. Instrumentation

Powder X−ray diffraction (PXRD) was performed on a Bruker AXS X−ray diffractometer with Cu Kα source. BET surface areas were determined from N_2 adsorption/desorption isotherms at 77 K using automatic volumetric adsorption equipment (Micromeritics ASAP2020) after pre−treatment under vacuum at 100 °C for 1000 min. Scanning Electron Microscope (SEM) images and energy dispersive spectra (EDS) were recorded on a Hitachi 800 Scanning Electron Microscope. Transmission Electron Microscope (TEM), High Resolution Transmission Electron Microscope (HRTEM) and Select Area Electron Diffraction (SAED) images were recorded on FEI Tecnai F20 Transmission Electron Microscope with operating voltage at 200 kV. High-angle annular dark-field Scanning Transmission Electron Microscopy (HAADF-STEM) images and EDS elemental mappings and High Resolution Scanning Transmission Electron Microscope (HRSTEM) images were acquired on a FEI Titan ST Microscope operated at 300 kV. Inductively coupled plasma atomic emission spectroscopy (ICP−AES) on an obin Yvon Horiba−Ultima 2 spectrometer system. Elemental Analyses (EA) were performed on a Vario MICRO analysis system. X−Ray Photoelectron Spectroscopy (XPS) analyses were performed using Kratos Axis DLD equipment. Fourier transform infrared spectra (FTIR) were recorded on a PerkinElmer high−resolution FT−IR. The ORR and OER tests were performed with a pine electrochemical analyser (AFMSRCE Electrode Rotator WaveDriver 20 Bipotentiostat/Galvanostat System, USA).

3. Synthetic procedures

Synthesis of ZIF−8 nanocrystals

ZIF−8 nanocrystals were prepared using a reported procedure with a slight modification.[1] In a typical synthesis, 4 g of 2−methylimidazole was dissolved in 60 mL of methanol (MeOH) to form a clear solution. 1.68 g of Zn(NO₃)₂·6H₂O in 20 mL MeOH was added into above solution followed by vigorous stirring for 1 h. The mixture was then incubated at room temperature without stirring. After 24 h, the product was isolated as a white powder by centrifugation and washed several times with deionized water and MeOH, and finally dried overnight under vacuum (yield = 1.06 g).

Electrochemical related calculations

All the current density in this work was calculated based on the geometrical area of rotating disk electrode. The numbers of electrons transferred (n) during ORR was calculated by Koutecky–Levich equation, at various electrode potentials:

$$1/j = 1/j_L + 1/j_K = 1/B\omega^{1/2} + 1/j_K \quad \text{(i)}$$

$$B = 0.62nFC_0D_0^{2/3}v^{-1/6} \quad \text{(ii)}$$

$$j_K = nFkC_0 \quad \text{(iii)}$$

where j is the measured current density; j_K and j_L are the kinetic and diffusion−limiting current densities, respectively; ω is the angular velocity of the disk (= 2πN, N is the linear rotation speed); n represents the overall number of electrons transferred in oxygen reduction; F is the Faraday constant (F = 96485 C mol⁻¹); C_0 is the bulk concentration of O₂ (1.2×10^{-6} mol cm⁻³); D_0 is the diffusion coefficient of O₂ in 0.1 M KOH electrolyte (1.9×10^{-5} cm²s⁻¹); v is the kinematics viscosity for electrolyte, and k is the electron−transferred rate constant.

4. Materials characterization

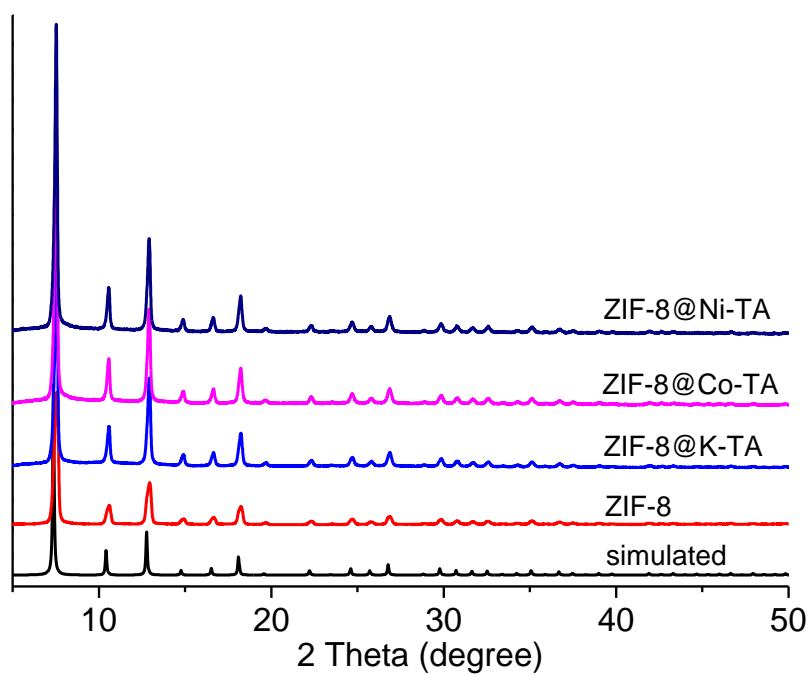## 4.1 Powder X–ray Diffraction (PXRD)

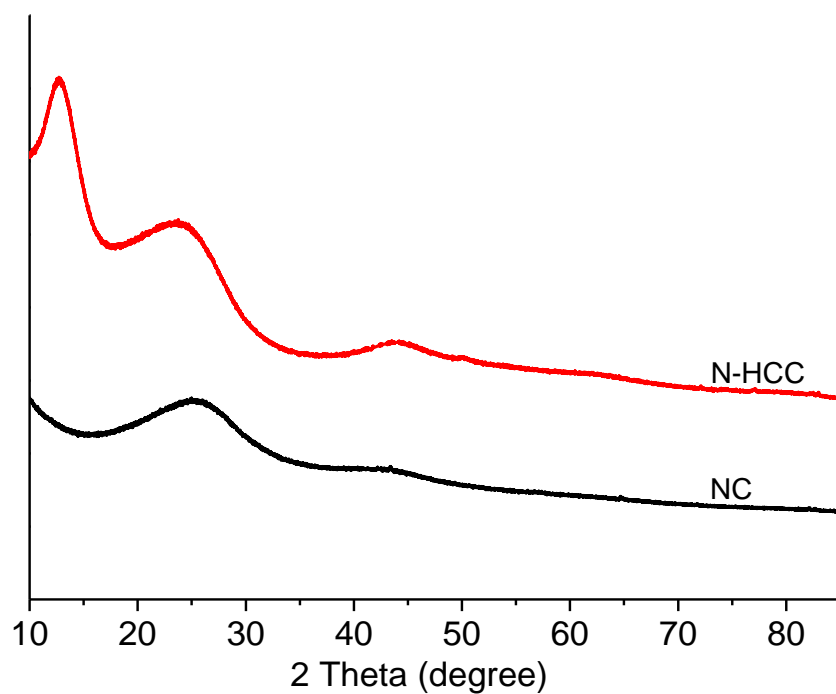**Fig. S1** PXRD patterns of as synthesized materials.

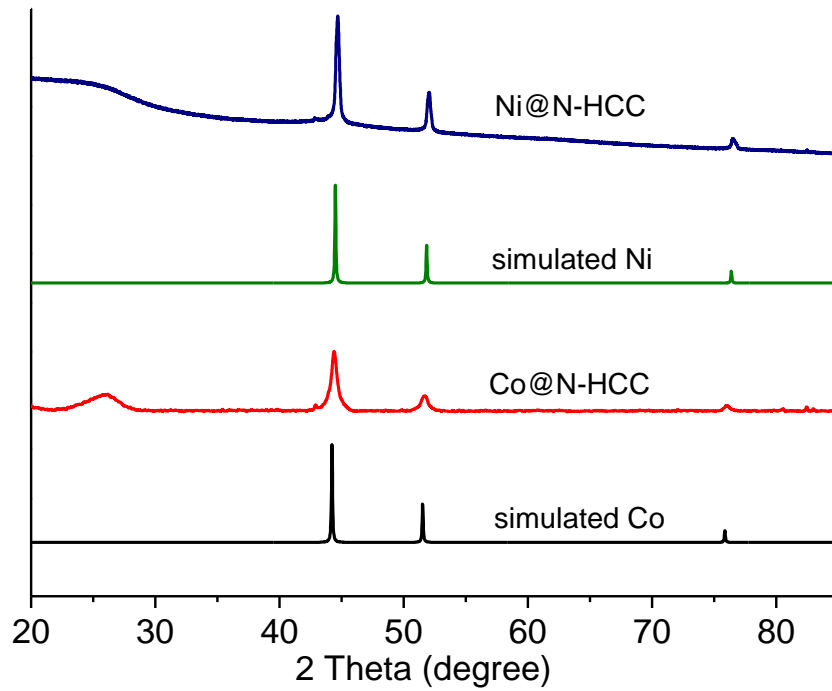**Fig. S2** PXRD patterns of as synthesized materials.

Fig. S3 PXRD patterns of as synthesized materials.
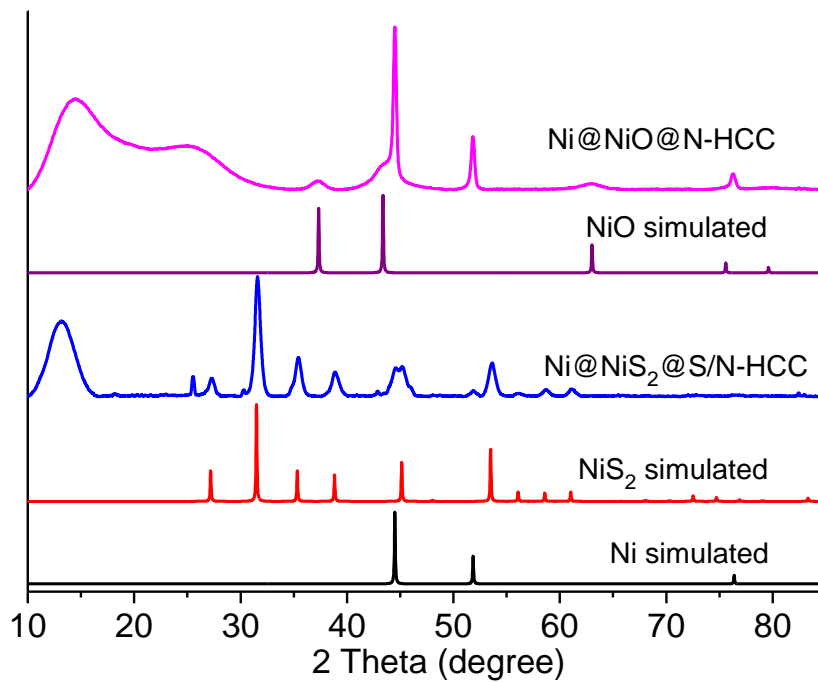

Fig. S4 PXRD patterns of as synthesized materials.

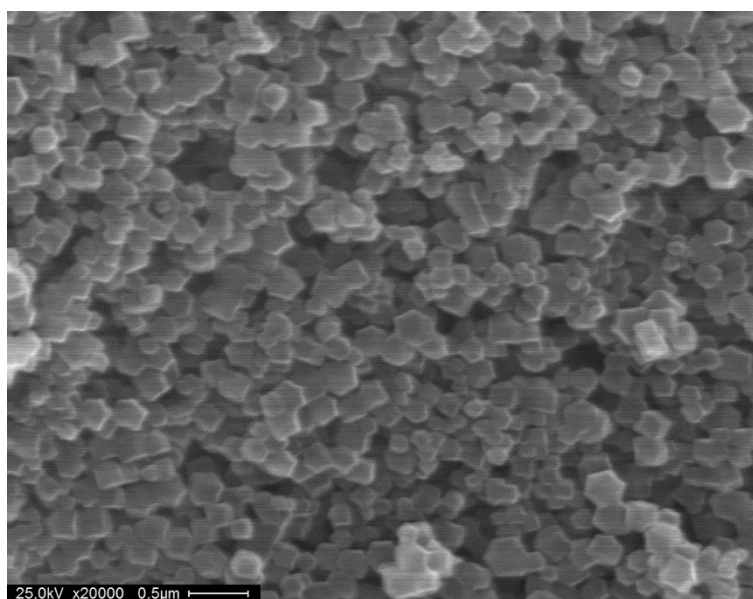**4.2 Scanning Electron Microscopy (SEM) and Transmission Electron Microscopy (TEM)**

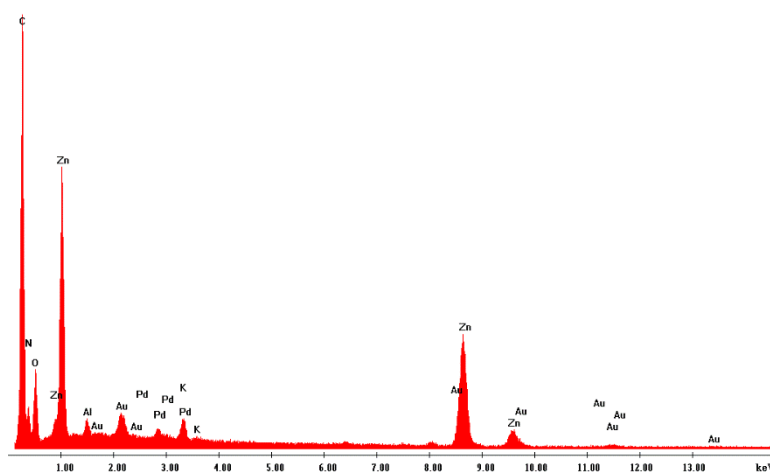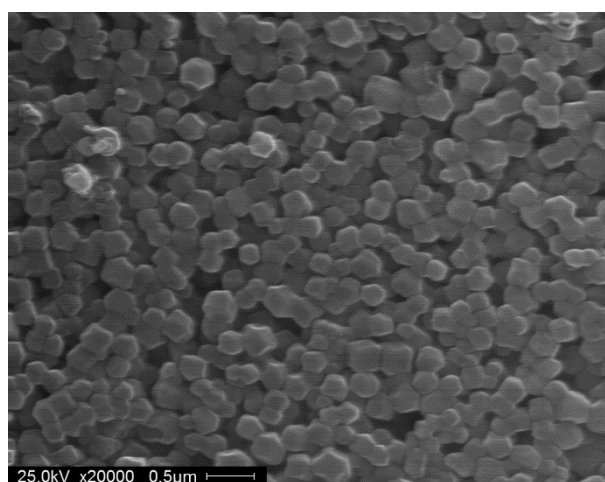**Fig. S5** SEM image of ZIF−8 nanocrystals.

Fig. S6 SEM image (left) and EDS spectrum (right) of ZIF−8@K−TA composite.
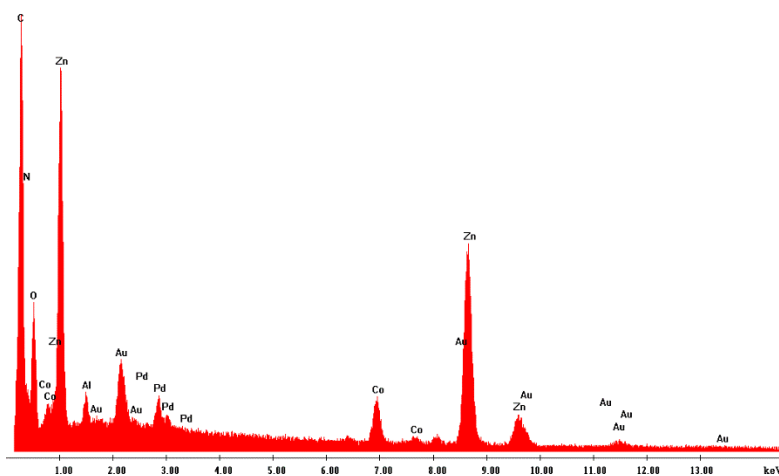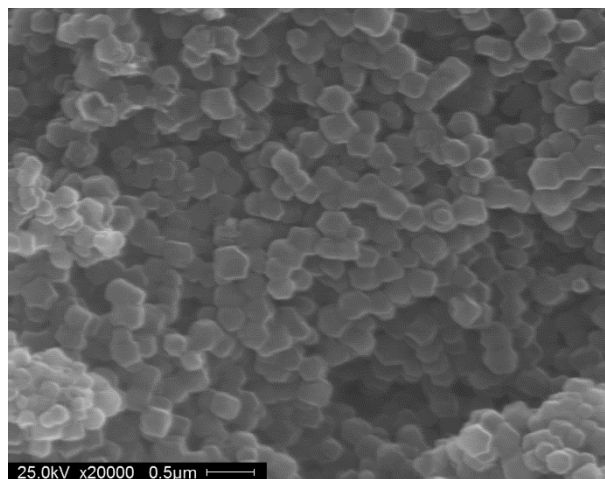
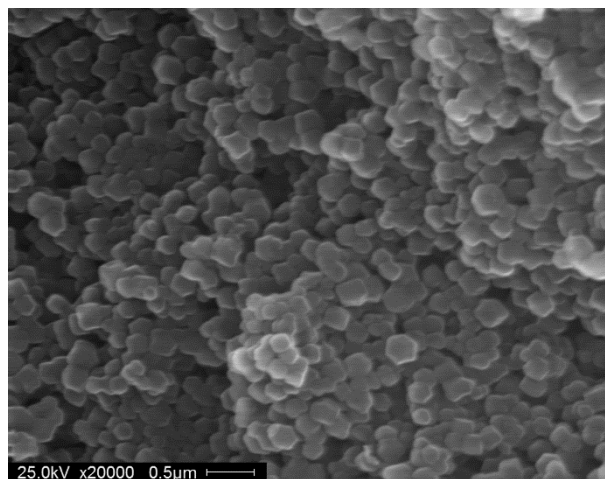**Fig. S7** SEM image (left) and EDS spectrum (right) of ZIF−8@Co−TA composite.
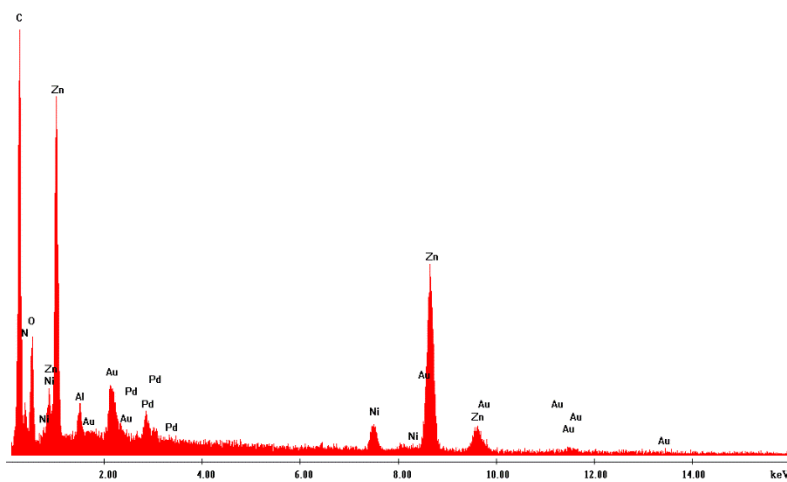
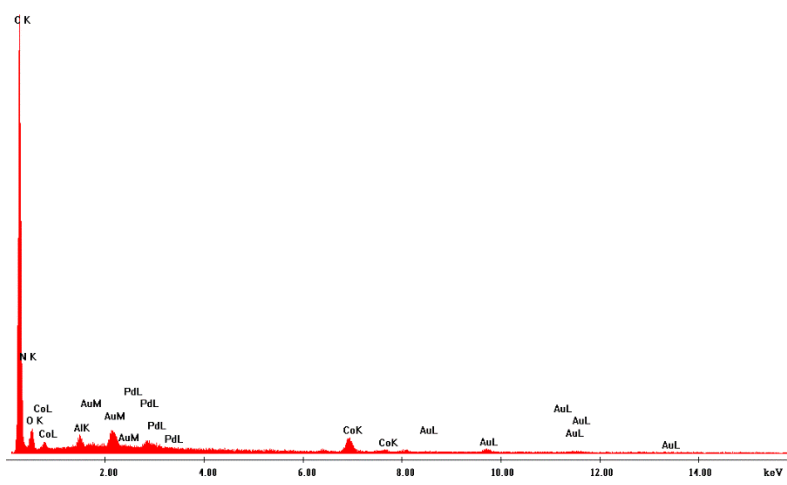**Fig. S8** SEM image (left) and EDS spectrum (right) of ZIF−8@Ni−TA composite.
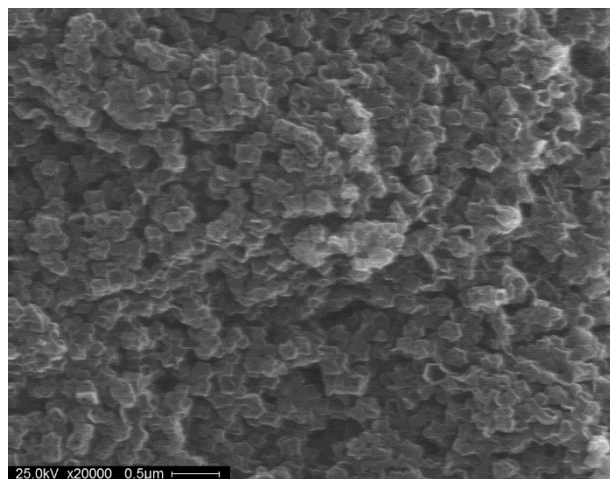
Fig. S9 SEM image (left) and EDS spectrum (right) of Co@N−HCC.
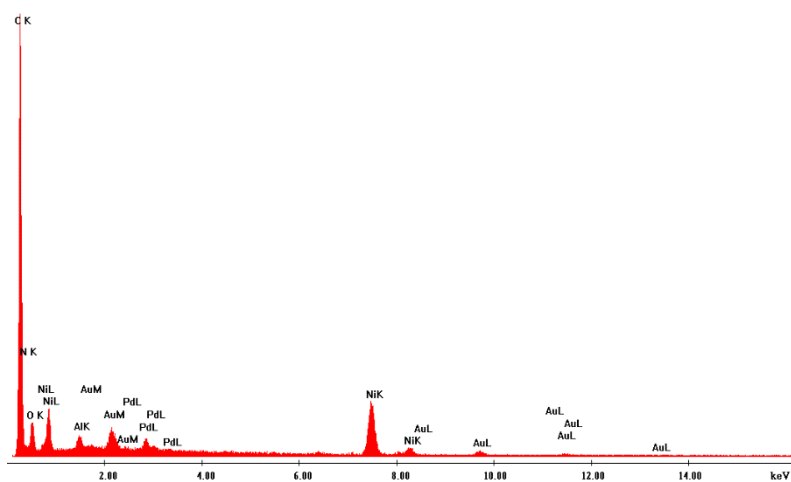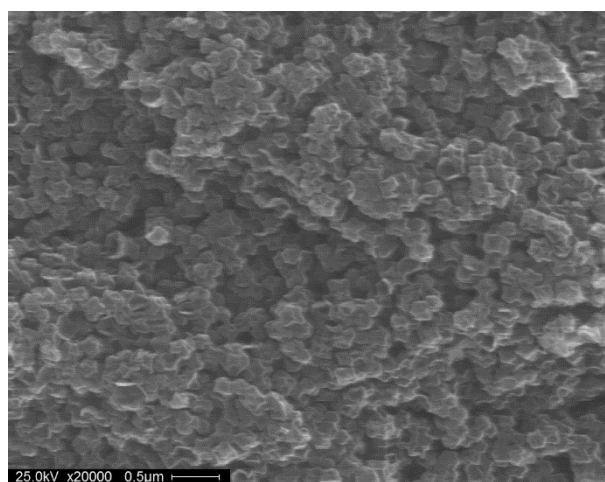
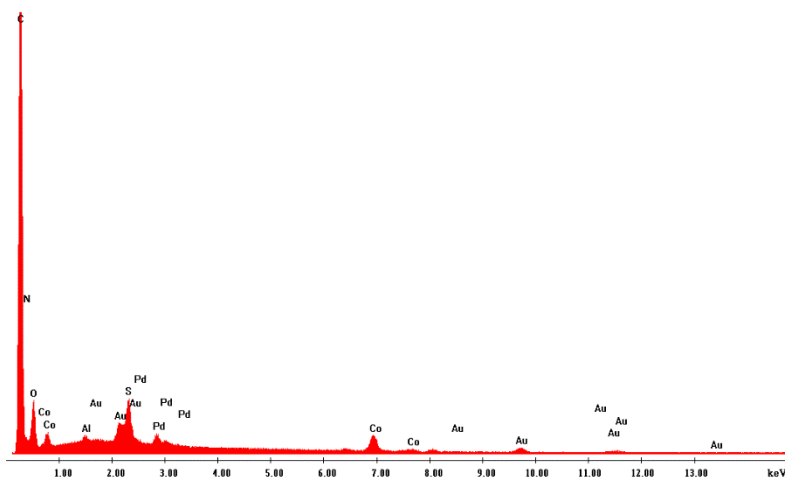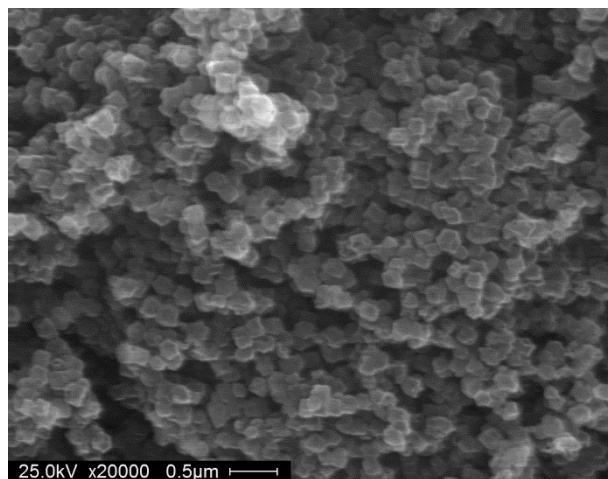**Fig. S10** SEM image (left) and EDS spectrum (right) of Ni@N−HCC.

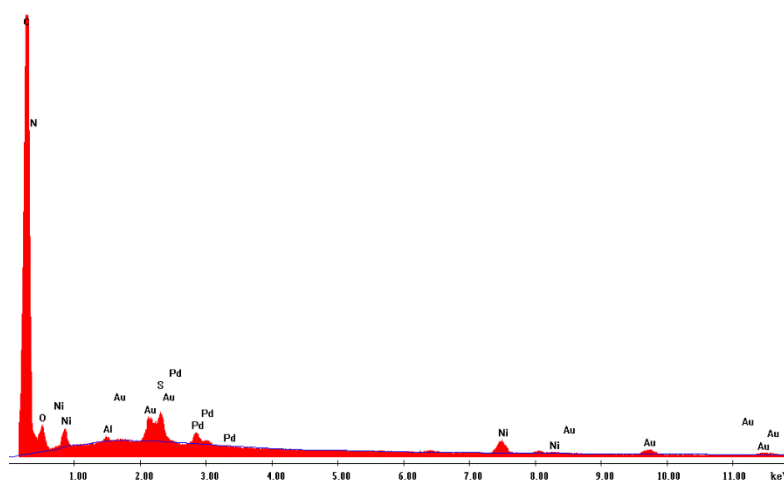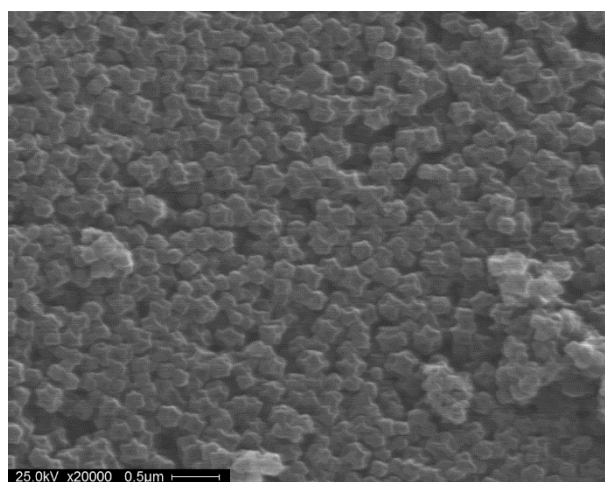**Fig. S11** SEM image (left) and EDS spectrum (right) of Co@CoS$_2$@S/N−HCC.

Fig. S12 SEM image (left) and EDS spectrum (right) of Ni@NiS$_2$@S/N−HCC.
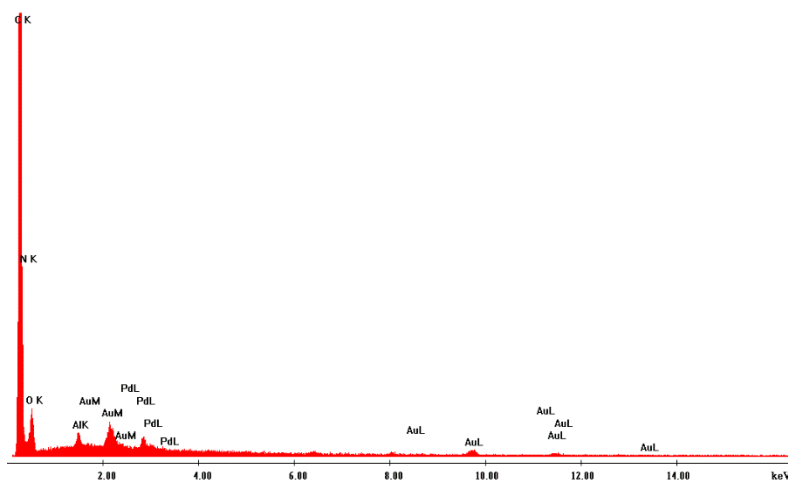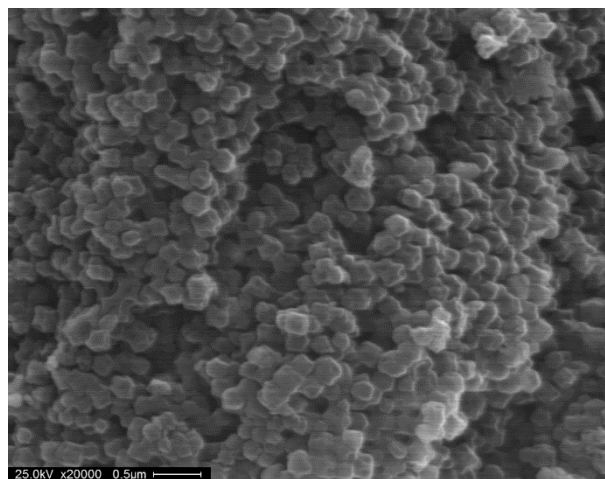
Fig. S13 SEM image (left) and EDS spectrum (right) of N−HCC.
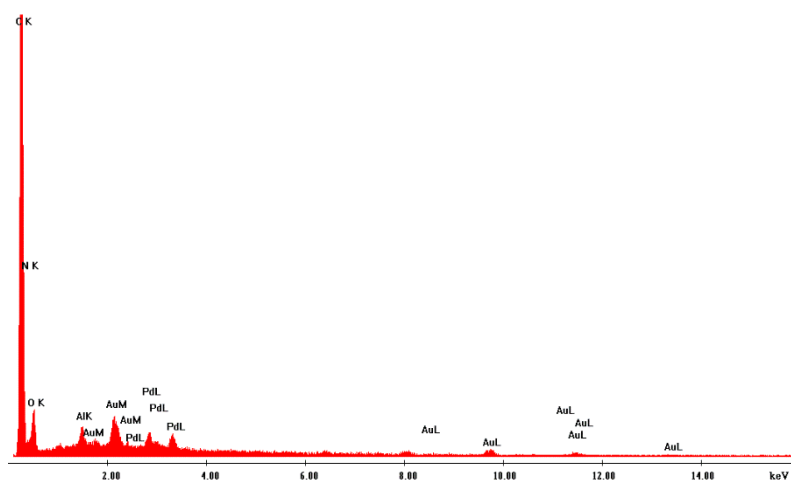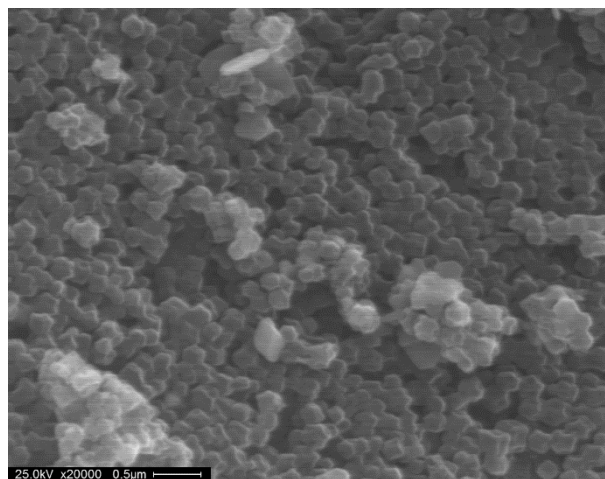
Fig. S14 SEM image (left) and EDS spectrum (right) of NC.
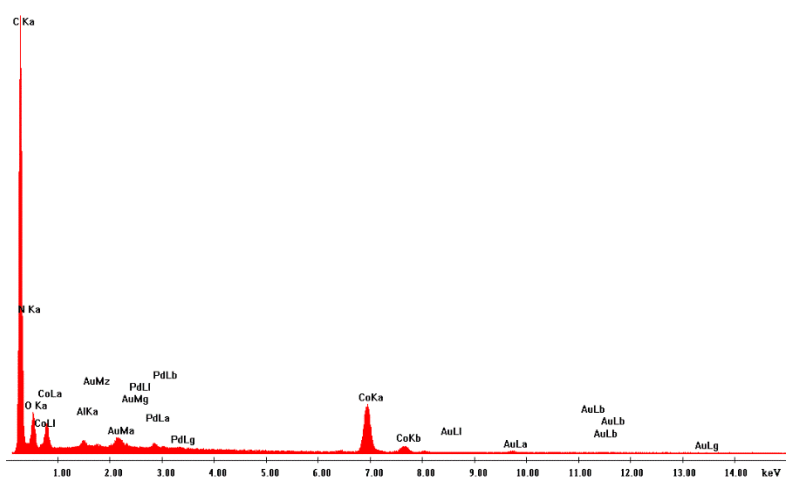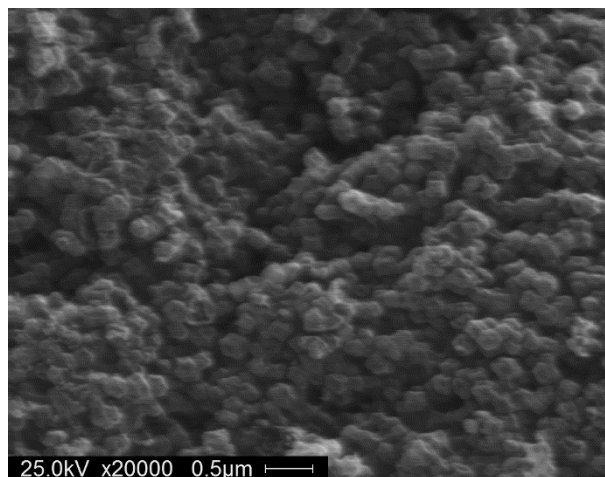
Fig. S15 SEM image (left) and EDS spectrum (right) of Co@Co$_3$O$_4$@N−HCC.
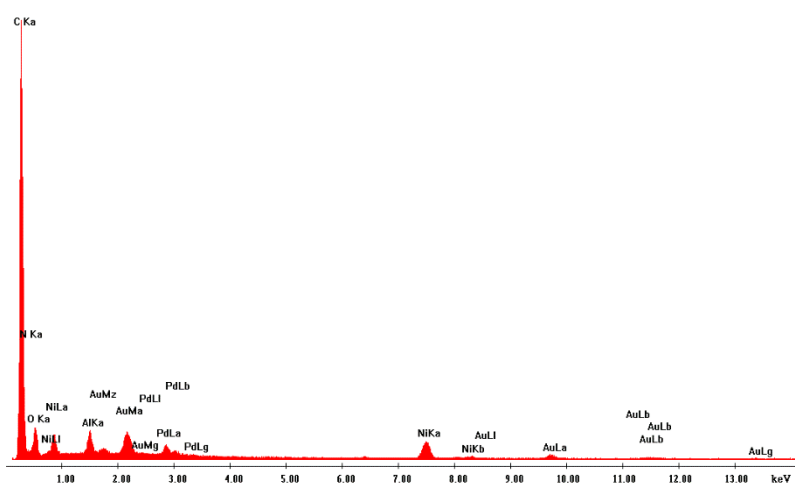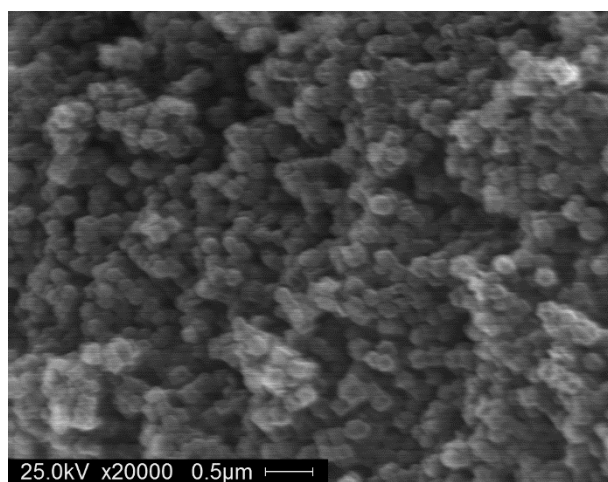
Fig. S16 SEM image (left) and EDS spectrum (right) of Ni@NiO@N−HCC.
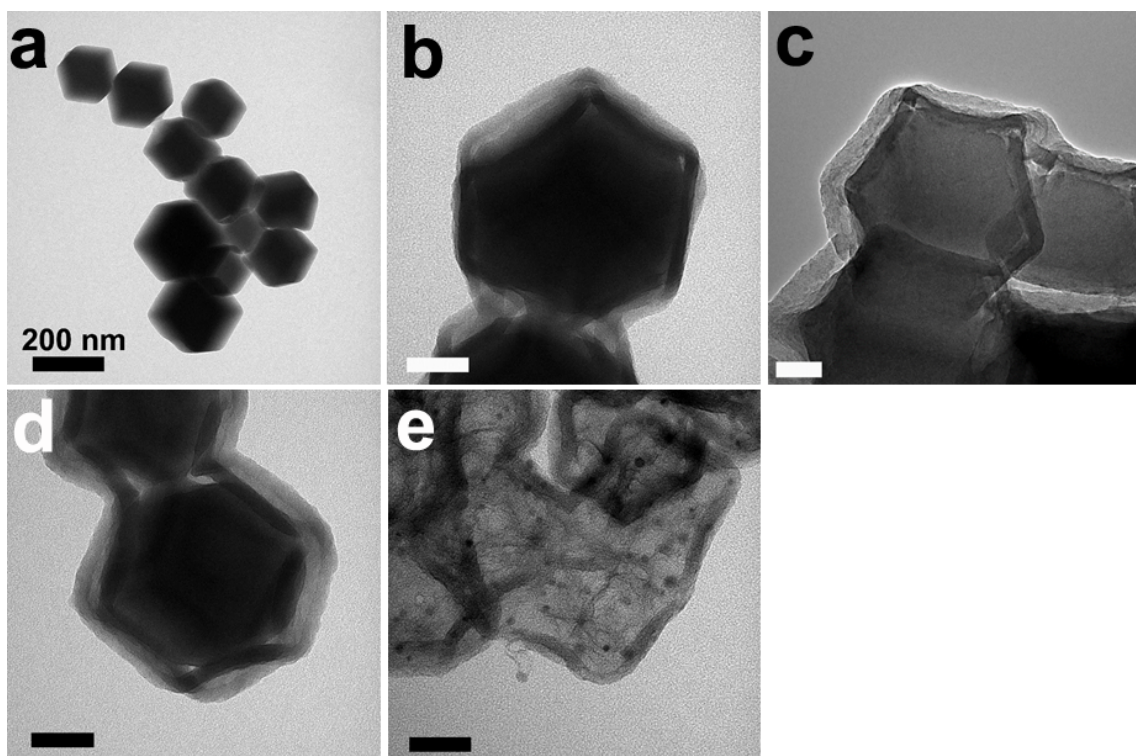
Fig. S17 TEM images as prepared materials: ZIF−8 nanocrystals (a); ZIF−8@K−TA (b); ZIF−8@Co−TA (c); ZIF−8@Ni−TA (d); Ni@N−HCC (e). The scale bars represent 50 nm, unless otherwise noted.
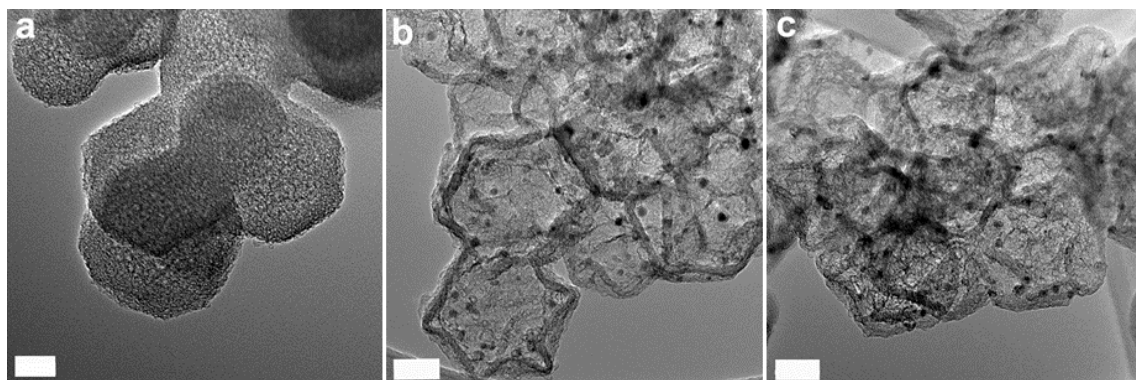
Fig. S18 TEM image of NC (a); low magnification of Co@Co$_3$O$_4$@N−HCC (b); low magnification of Ni@NiO@N−HCC (c). The scale bars represent 50 nm.
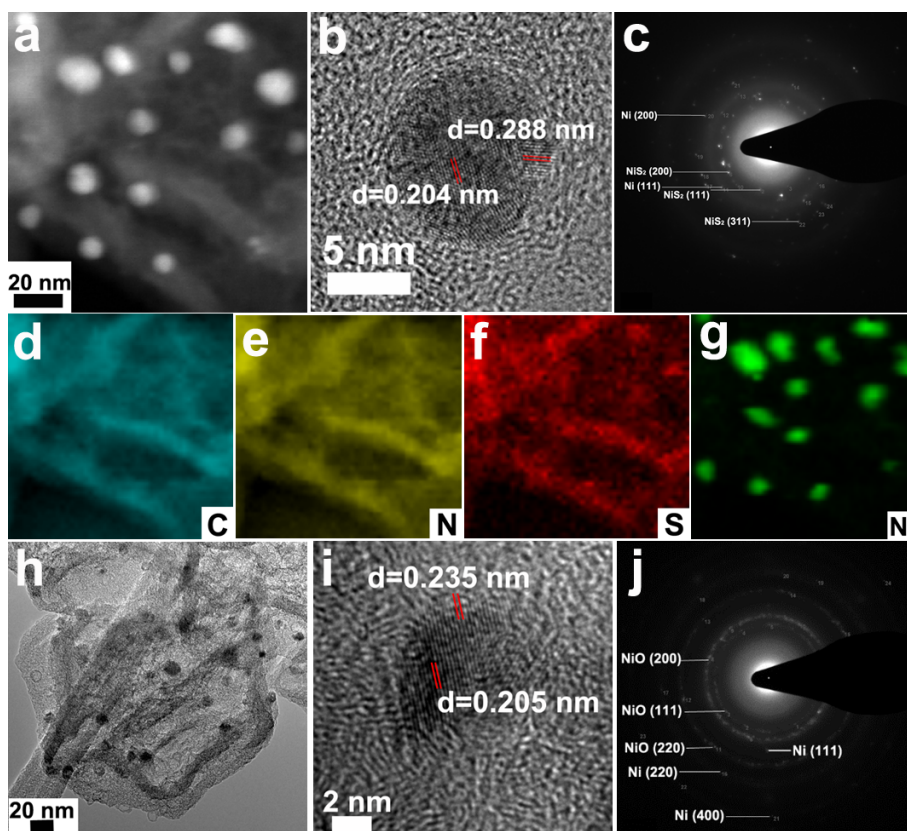
Fig. S19 (a) HAADF−STEM image of Ni@NiS$_2$@S/N−HCC; (b) HRTEM image showing an individual Ni@NiS$_2$

core−shell nanoparticle; (c) SAED pattern of Ni@NiS$_2$@S/N−HCC; (d−g) EDS elemental (C, N, S and Ni)

mapping of Ni@NiS$_2$@S/N−HCC; (h) TEM image of Ni@NiO@N−HCC; (i) HRTEM image showing an

individual Ni@NiO core−shell nanoparticle; (j) SAED pattern of Ni@NiO@N−HCC.
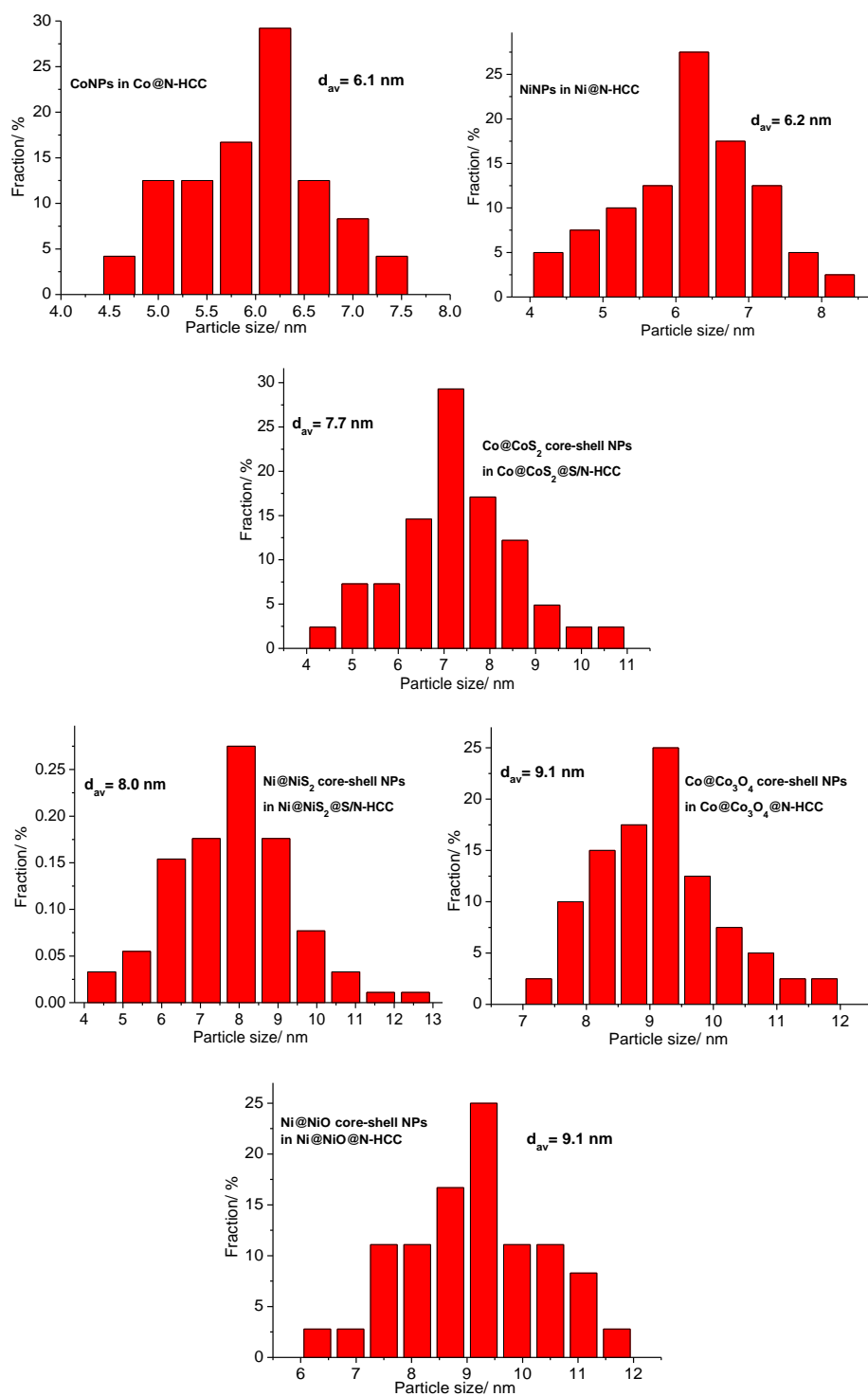
Fig. S20 Histograms of nanoparticle and average particle sizes for materials.

4.3 Nitrogen sorption measurements, pore size analysis and surface area calculations:
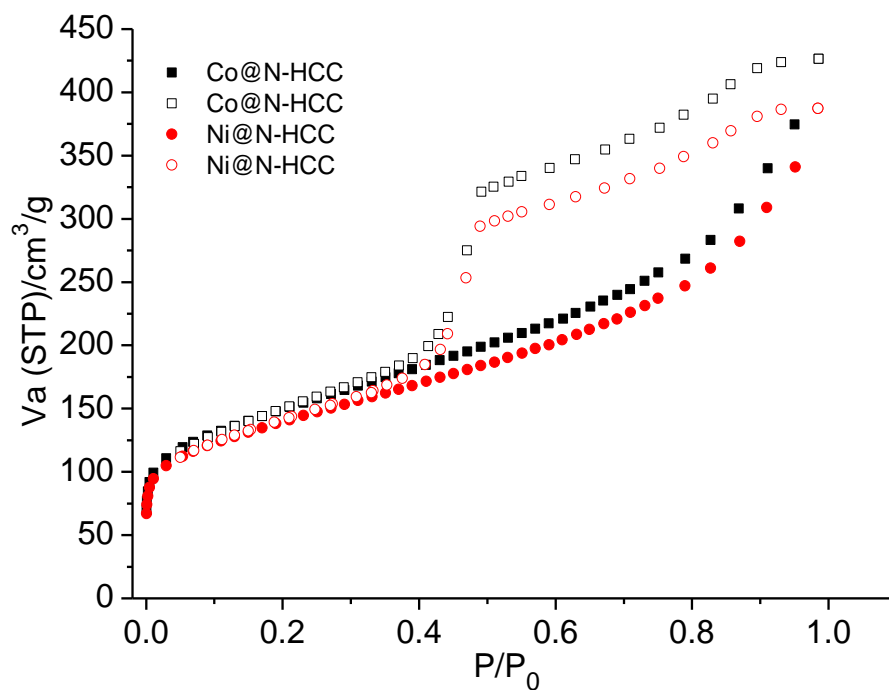
Fig. S21 N$_2$ adsorption (filled symbols) and desorption (open symbols) isotherms measured at 77 K.
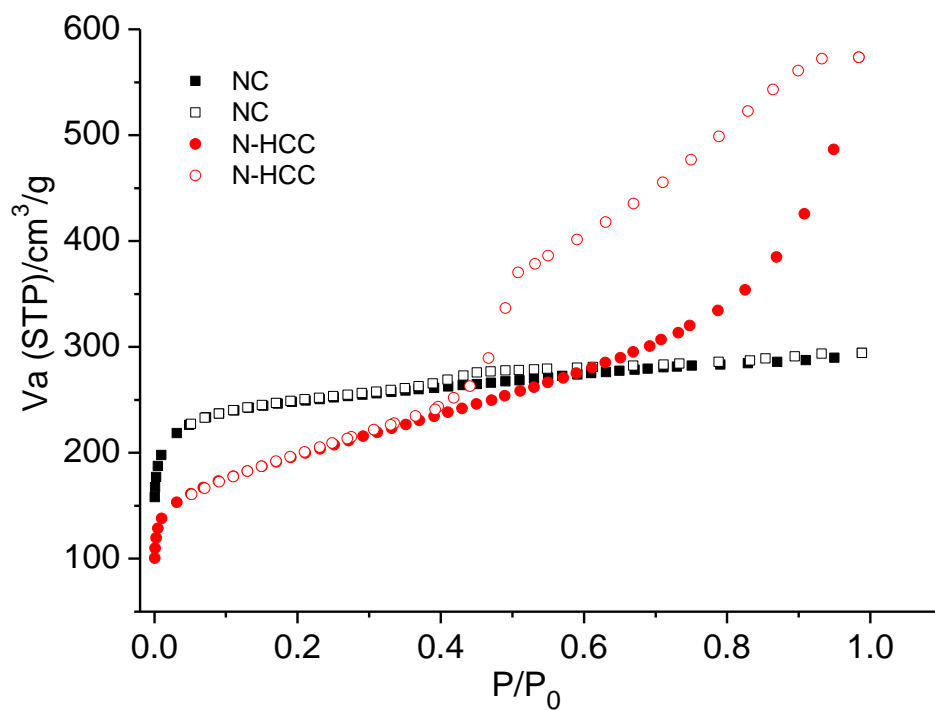
Fig. S22 N$_2$ adsorption (filled symbols) and desorption (open symbols) isotherms measured at 77 K.
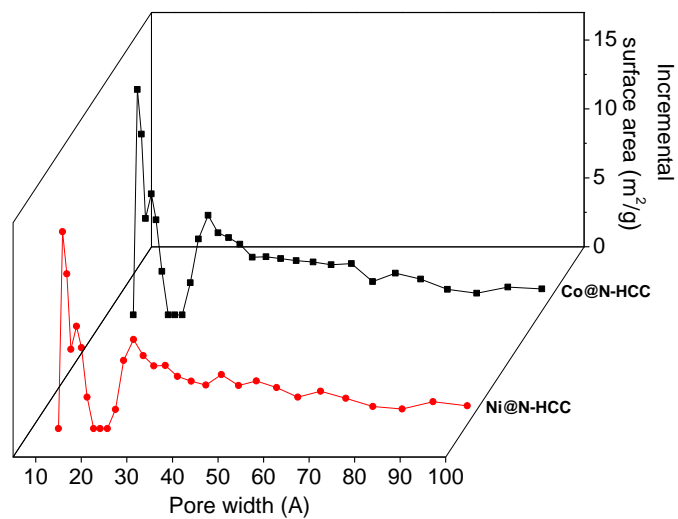
Fig. S23 Pore size distribution plots calculated using a DFT method from N_2 isotherms measured at 77 K.
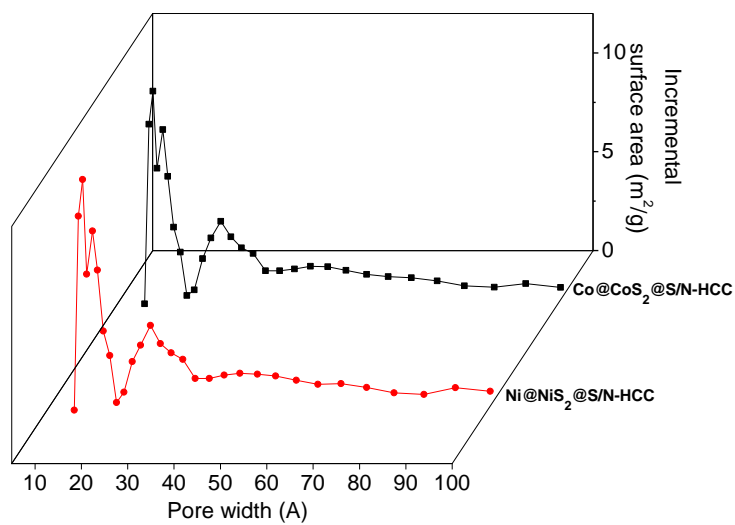
Fig. S24 Pore size distribution plots calculated using a DFT method from N_2 isotherms measured at 77 K.
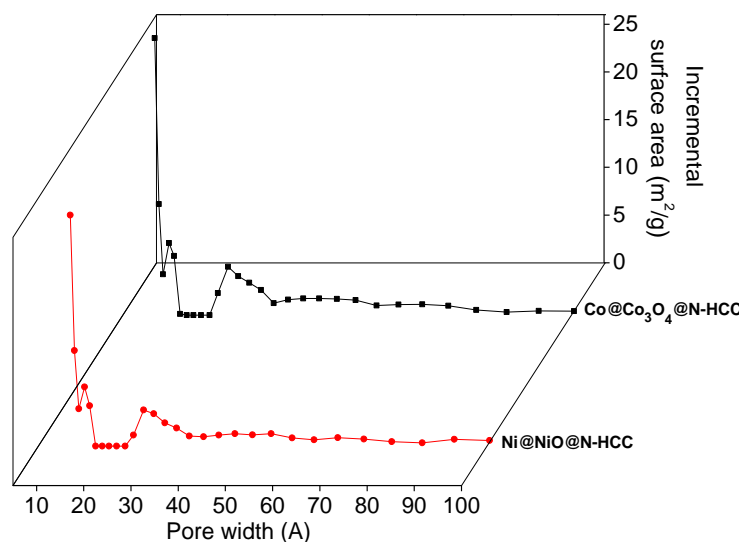
Fig. S25 Pore size distribution plots calculated using a DFT method from N_2 isotherms measured at 77 K.

4.4 X−Ray Photoelectron Spectroscopy (XPS)
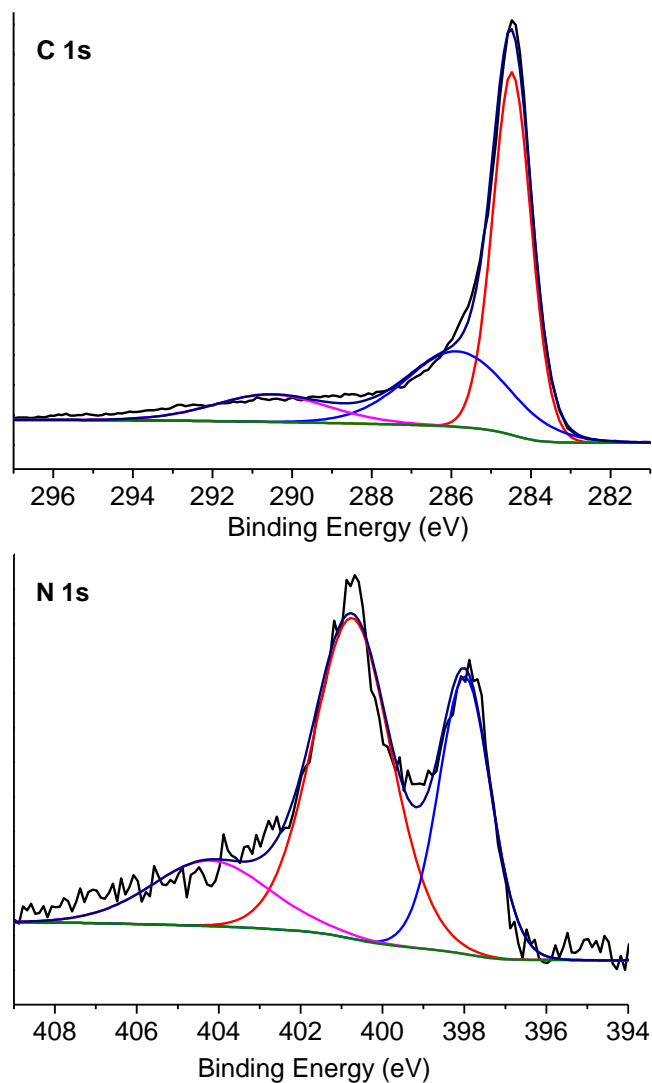
Fig. S26 XPS spectra of N−HCC.
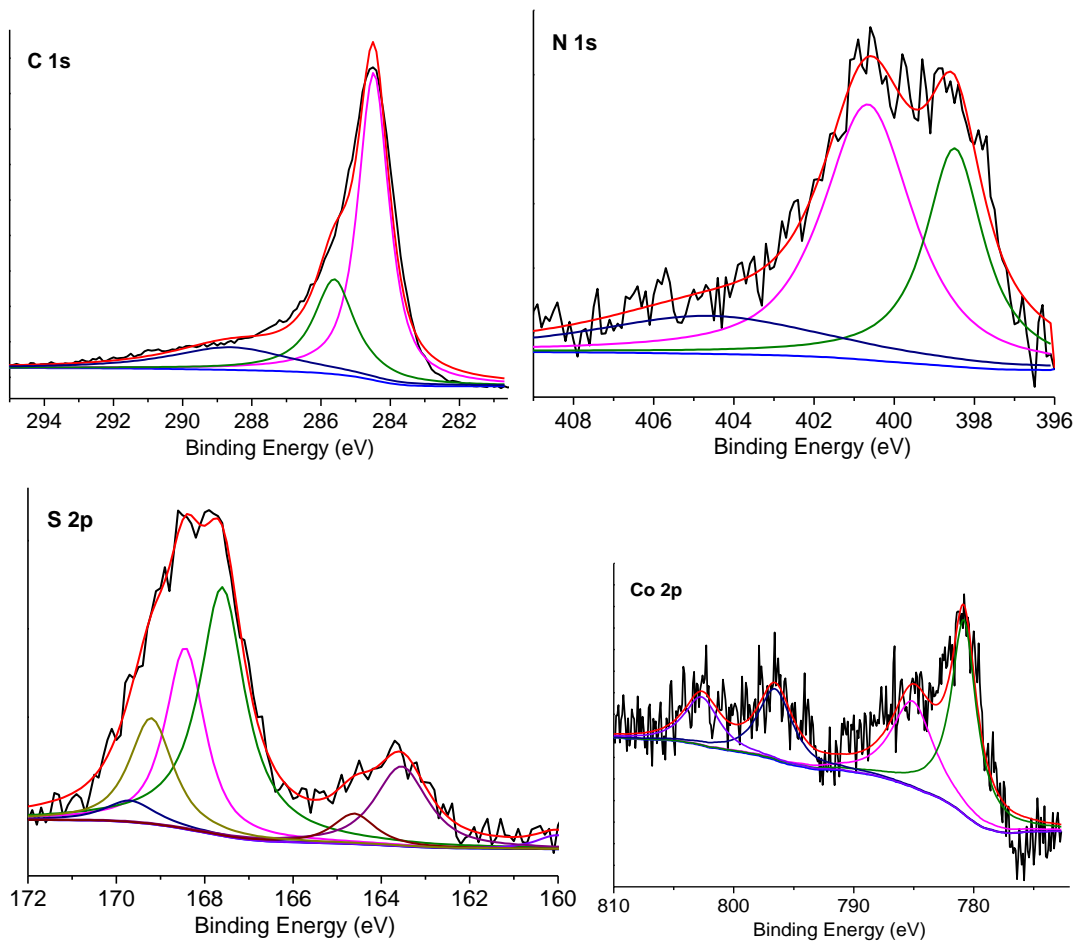
Fig. S27 XPS spectra of Co@CoS$_2$@S/N−HCC.
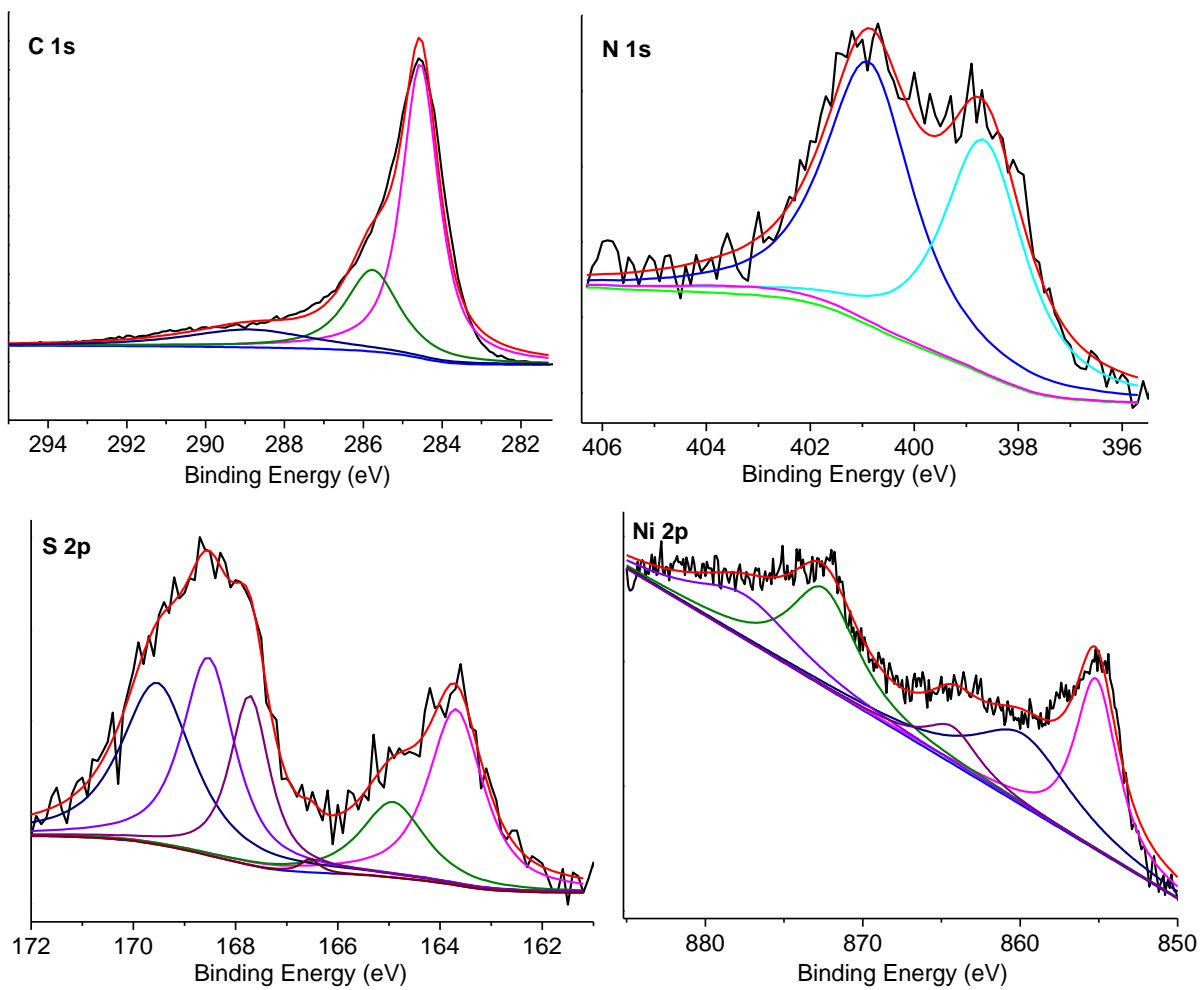
Fig. S28 XPS spectra of Ni@NiS$_2$@S/N−HCC.
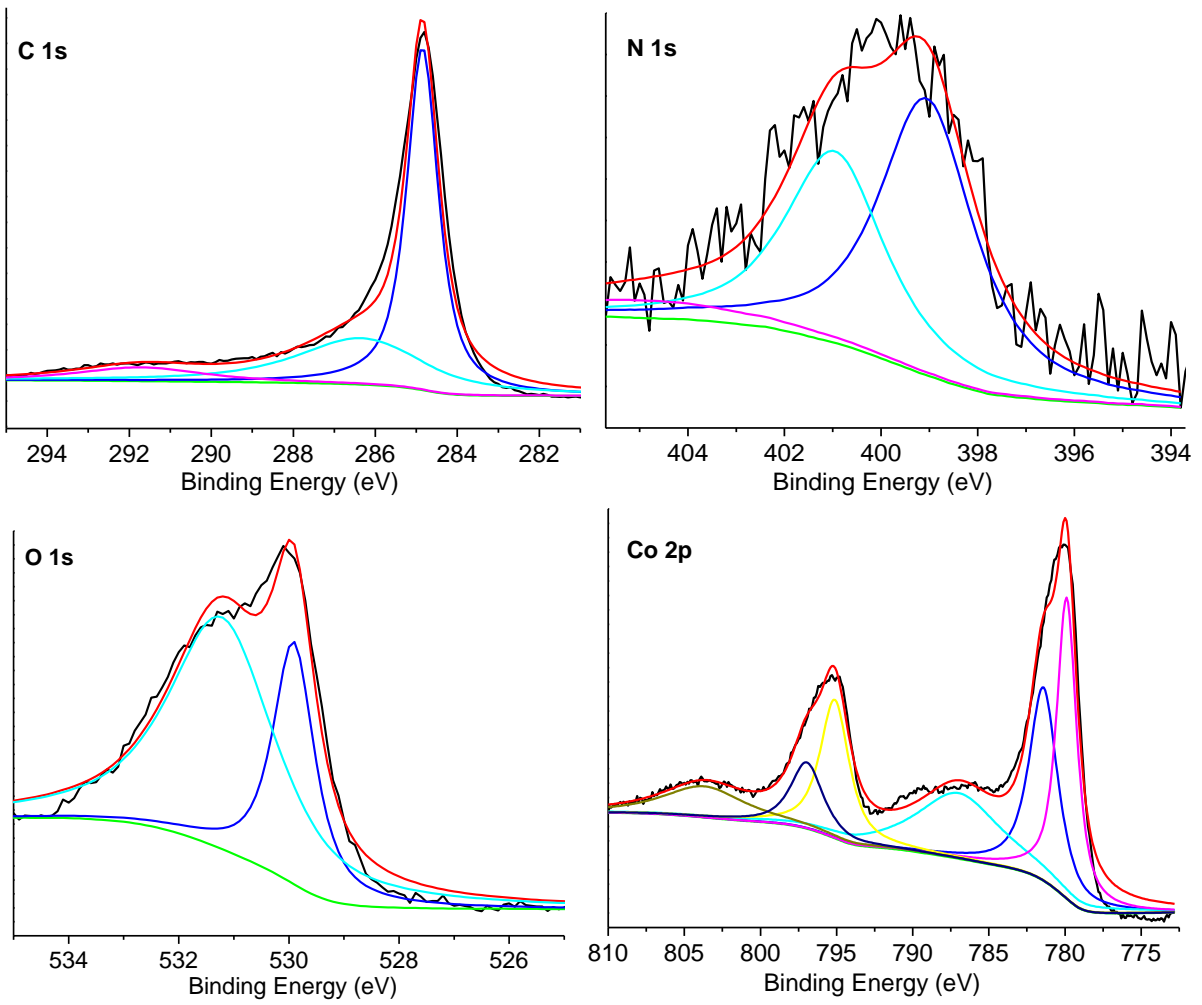
Fig. S29 XPS spectra of Co@Co$_3$O$_4$@N–HCC.
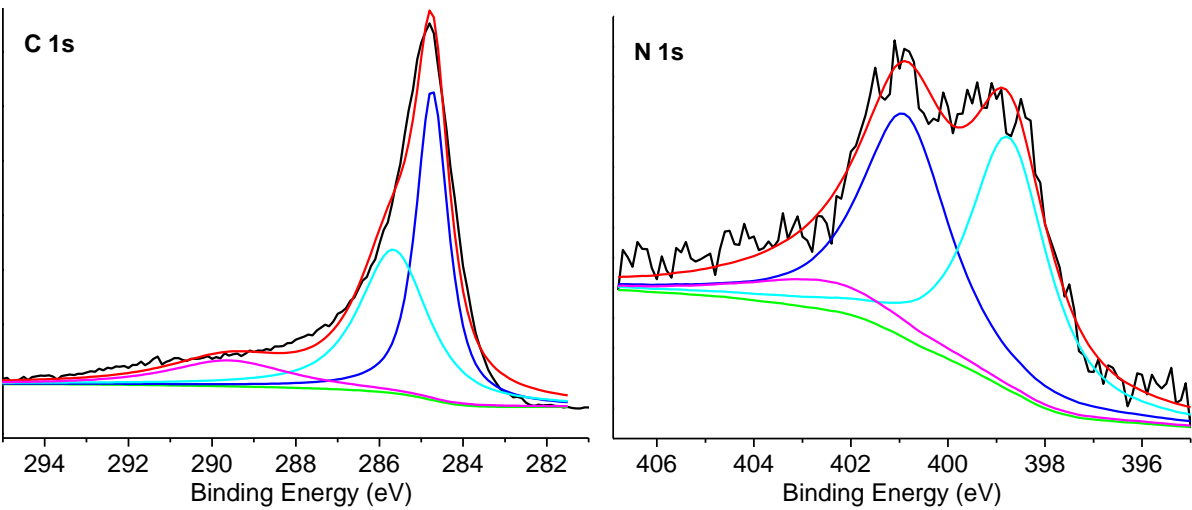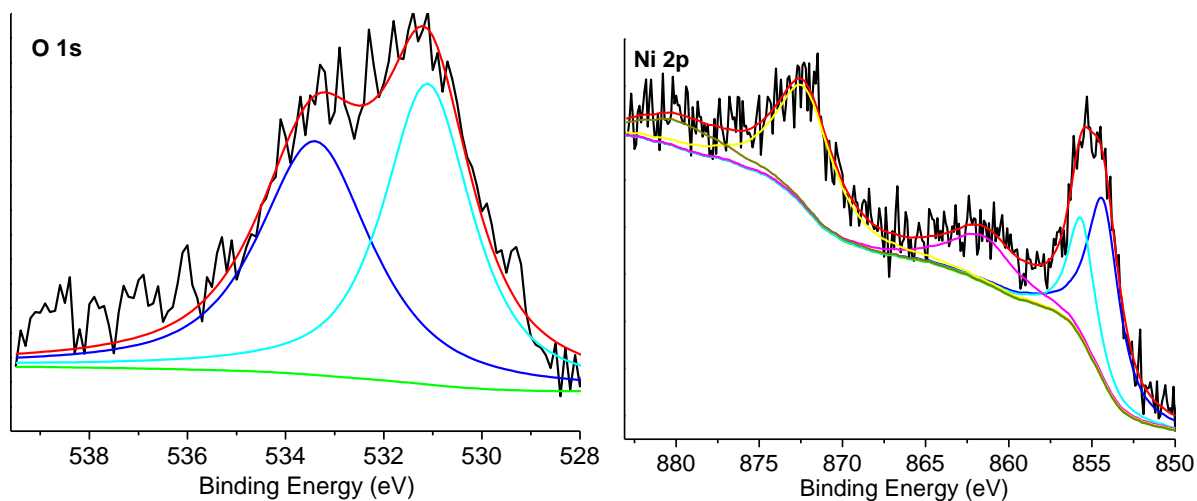
Fig. S30 XPS spectra of Ni@NiO@N−HCC.

4.5 Fourier Transform Infrared Spectrophotometry (FT−IR)
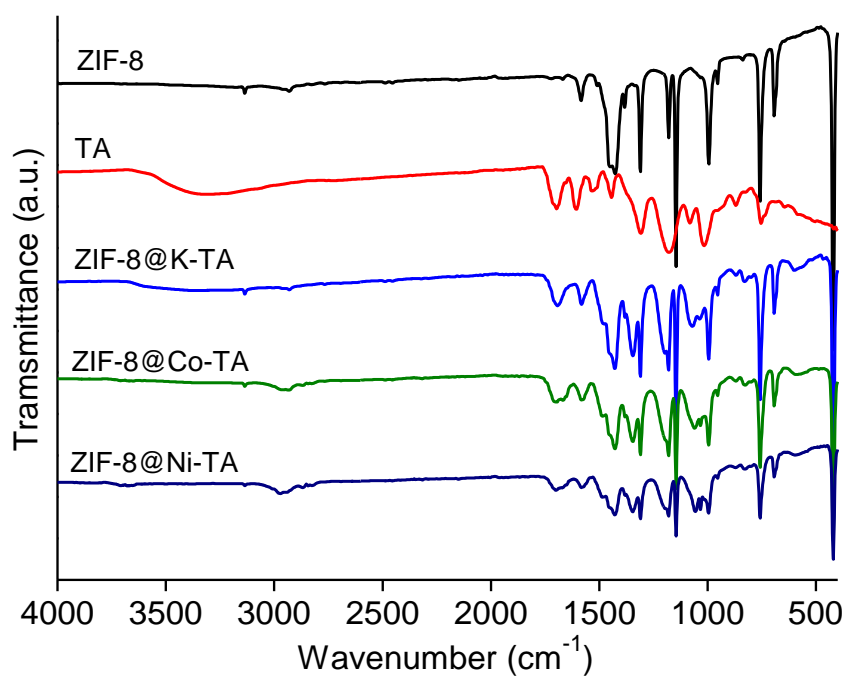
Fig. S31 FTIR spectra of materials.

4.6 Oxygen Reduction Reaction (ORR)
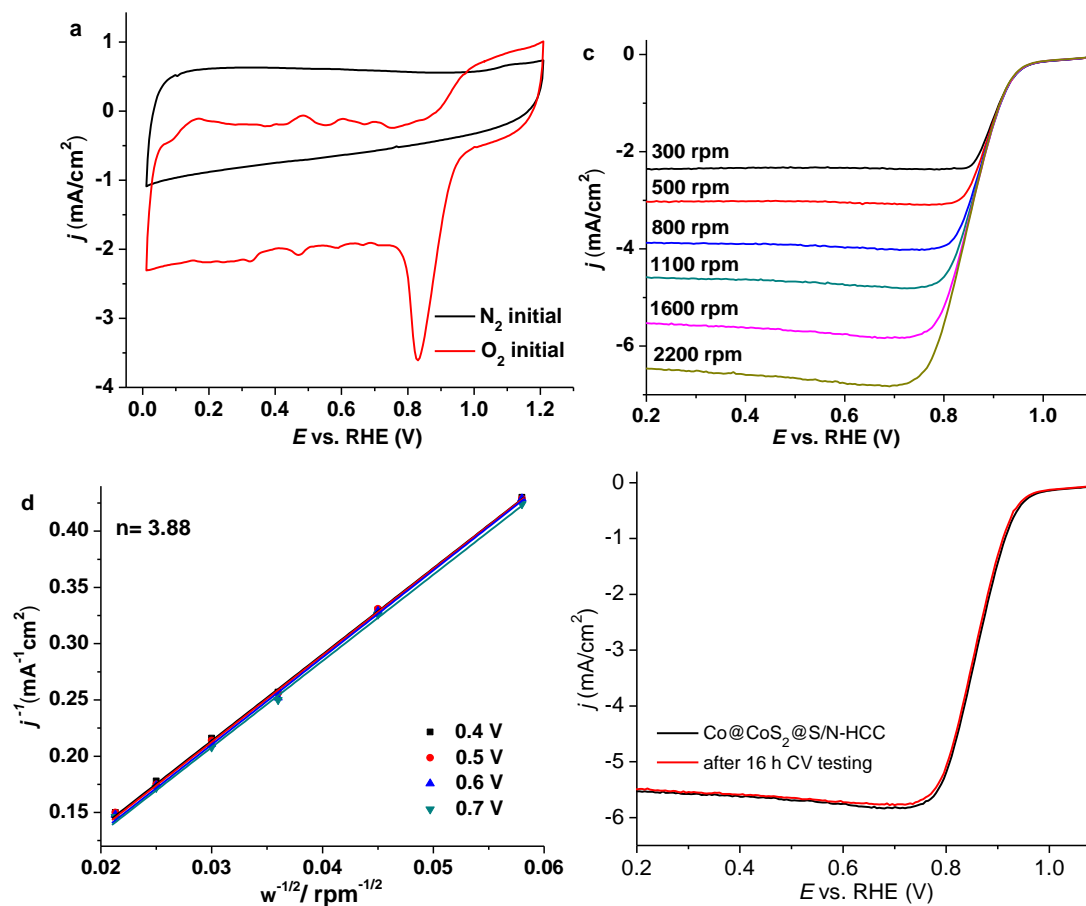
Fig. S32 (a) CV curves of Co@CoS$_2$@S/N−HCC in aqueous 0.1 M KOH solution with a scan speed of 20 mV/s; (b) LSV curves of Co@CoS$_2$@S/N−HCC in O$_2$−saturated 0.1 M KOH solution with different rotating rates; (c) K−L plots for Co@CoS$_2$@S/N−HCC calculated from the LSV curves and the electron transfer number (n); (d) The polarization curves of Co@CoS$_2$@S/N−HCC sample before and after 16 h CV testing with a san rate of 50 mV/s in a 0.1 M KOH solution.
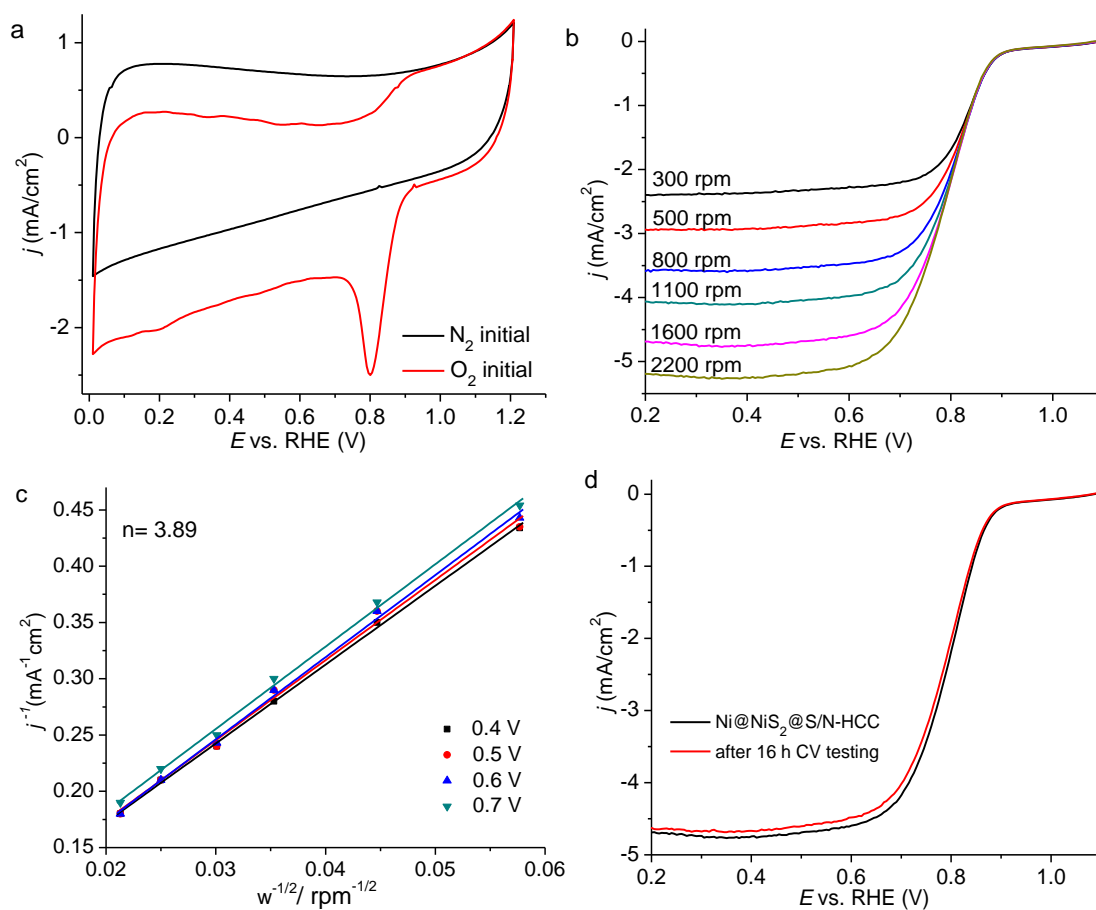
Fig. S33 CV curves of Ni@NiS$_2$@S/N−HCC in 0.1 M KOH solution with a scan speed of 20 mV/s (a); LSV curves of Ni@NiS$_2$@S/N−HCC in O$_2$−saturated 0.1 M KOH solution with the different rotating speeds (b); K−L plots for Ni@NiS$_2$@S/N−HCC calculated from LSV curves and the electron transfer number (c); The polarization curves of Ni@NiS$_2$@S/N−HCC sample before and after 16 h CV testing with a san rate of 50 mV/s in a 0.1 M KOH solution (d).
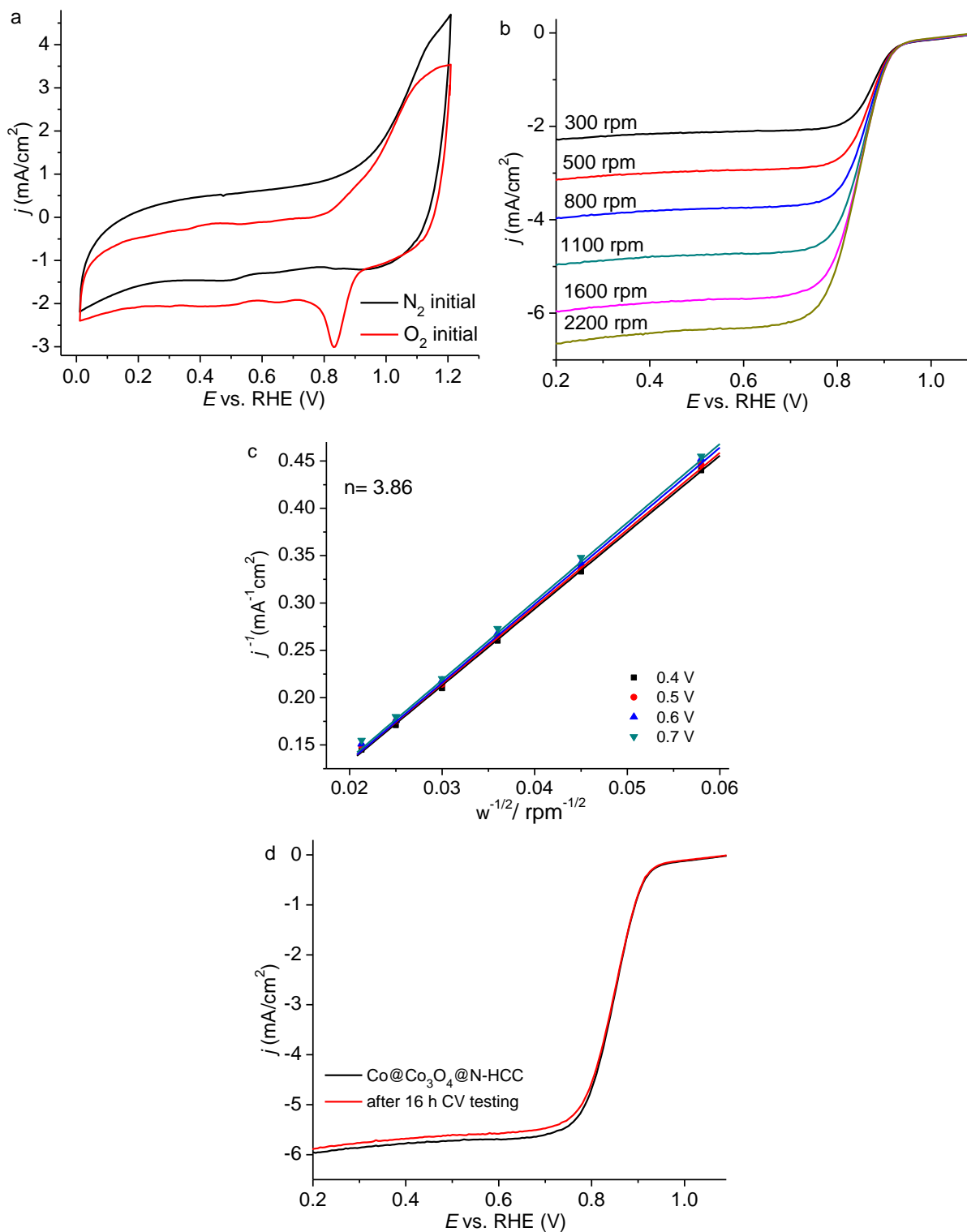
Fig. S34 CV curves of Co@Co$_3$O$_4$@N−HCC in 0.1 M KOH solution with a scan speed of 20 mV/s (a); LSV curves of Co@Co$_3$O$_4$@N−HCC in O$_2$−saturated 0.1 M KOH solution with the different rotating speeds (b); K−L plots for Co@Co$_3$O$_4$@N−HCC calculated from LSV curves and the electron transfer number (c); The polarization curves of Co@Co$_3$O$_4$@N−HCC sample before and after 16 h CV testing with a san rate of 50 mV/s in a 0.1 M KOH solution (d).
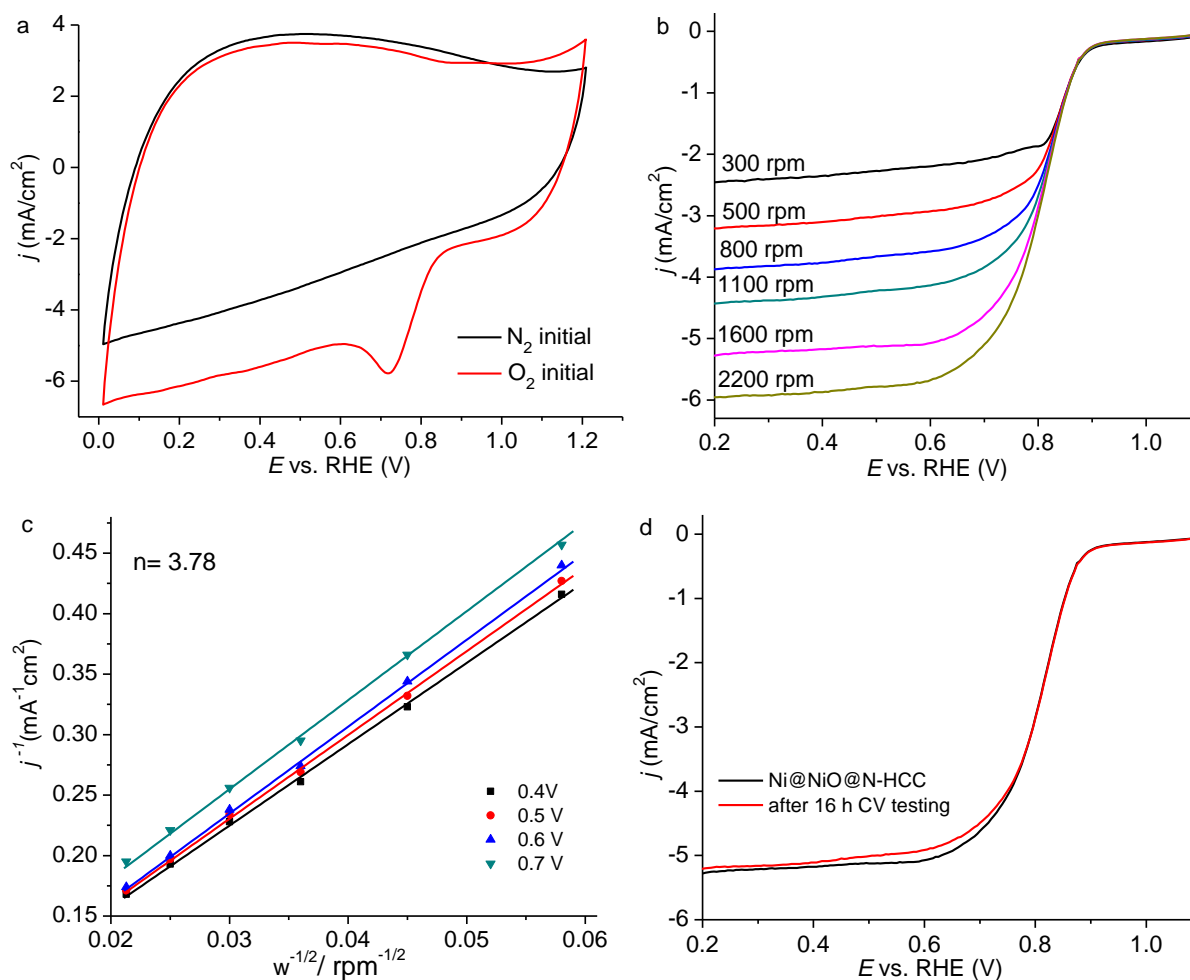
Fig. S35 CV curves of Ni@NiO@N–HCC in 0.1 M KOH solution with a scan speed of 20 mV/s (a); LSV curves of Ni@NiO@N–HCC in O_2–saturated 0.1 M KOH solution with the different rotating speeds (b); K–L plots for Ni@NiO@N–HCC calculated from LSV curves and the electron transfer number (c); The polarization curves of Ni@NiO@N–HCC sample before and after 16 h CV testing with a san rate of 50 mV/s in a 0.1 M KOH solution (d).
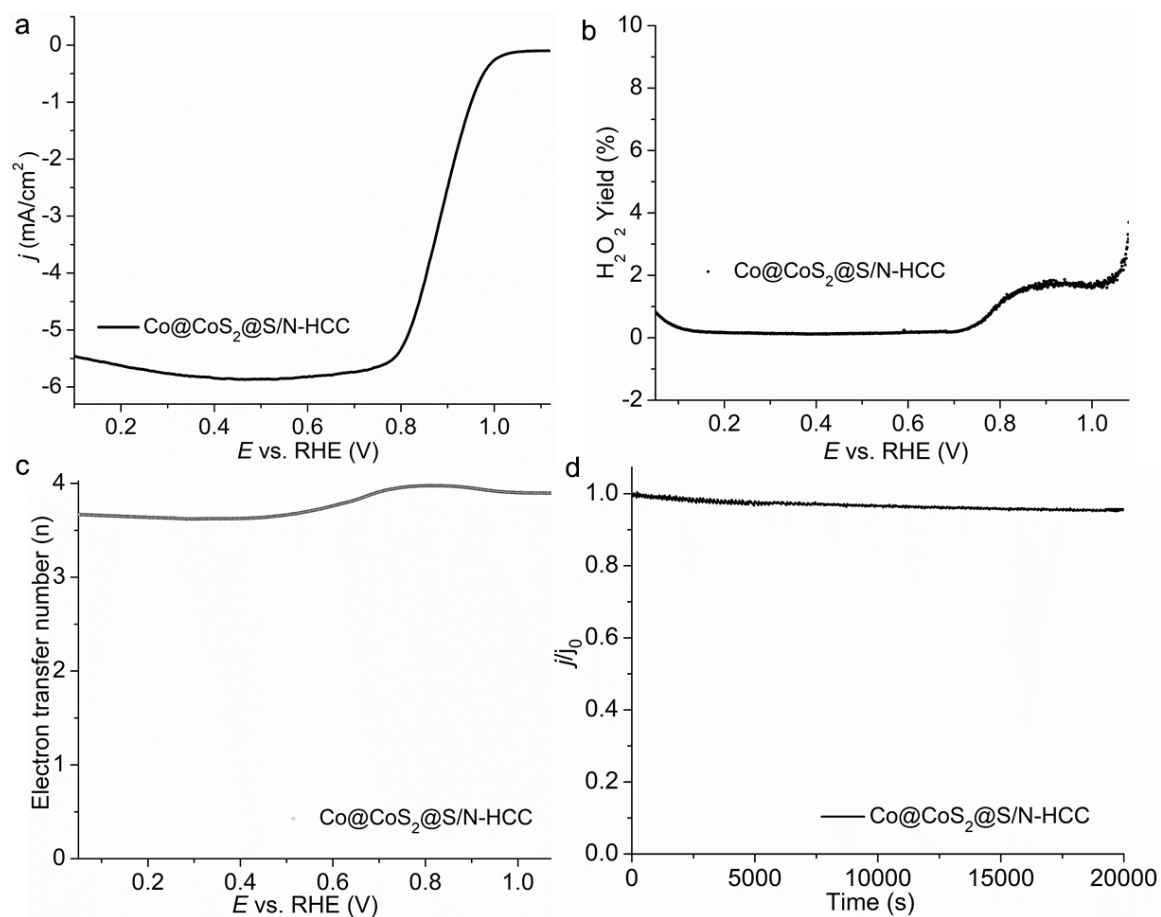
Fig. S36 LSV cure of Co@CoS$_2$@S/N−HCC in 0.1 M KOH by RRDE technique (a); H$_2$O$_2$ yield of Co@CoS$_2$@S/N−HCC in 0.1 M KOH (b); electron-transfer number of Co@CoS$_2$@S/N−HCC by RRDE technique (c); Chronoamperometry curve of Co@CoS$_2$@S/N−HCC at 0.45 V vs. RHE in 0.1 M KOH (d).

4.7 Oxygen Evolution Reaction (OER)
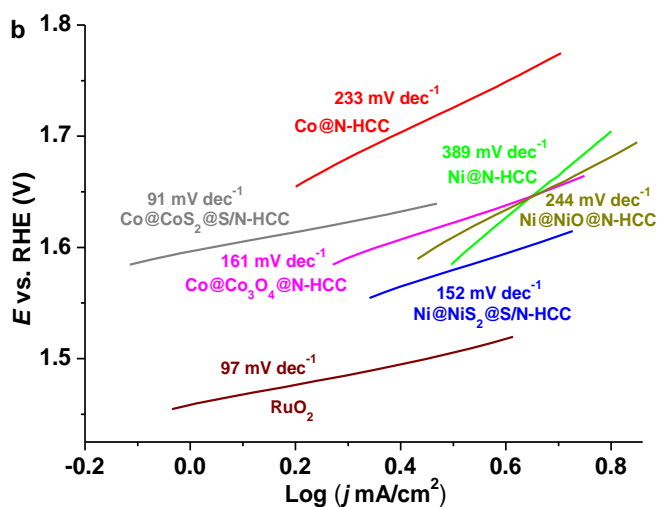
Fig. S37 Tafel plots calculated from polarization curves of different catalysts.
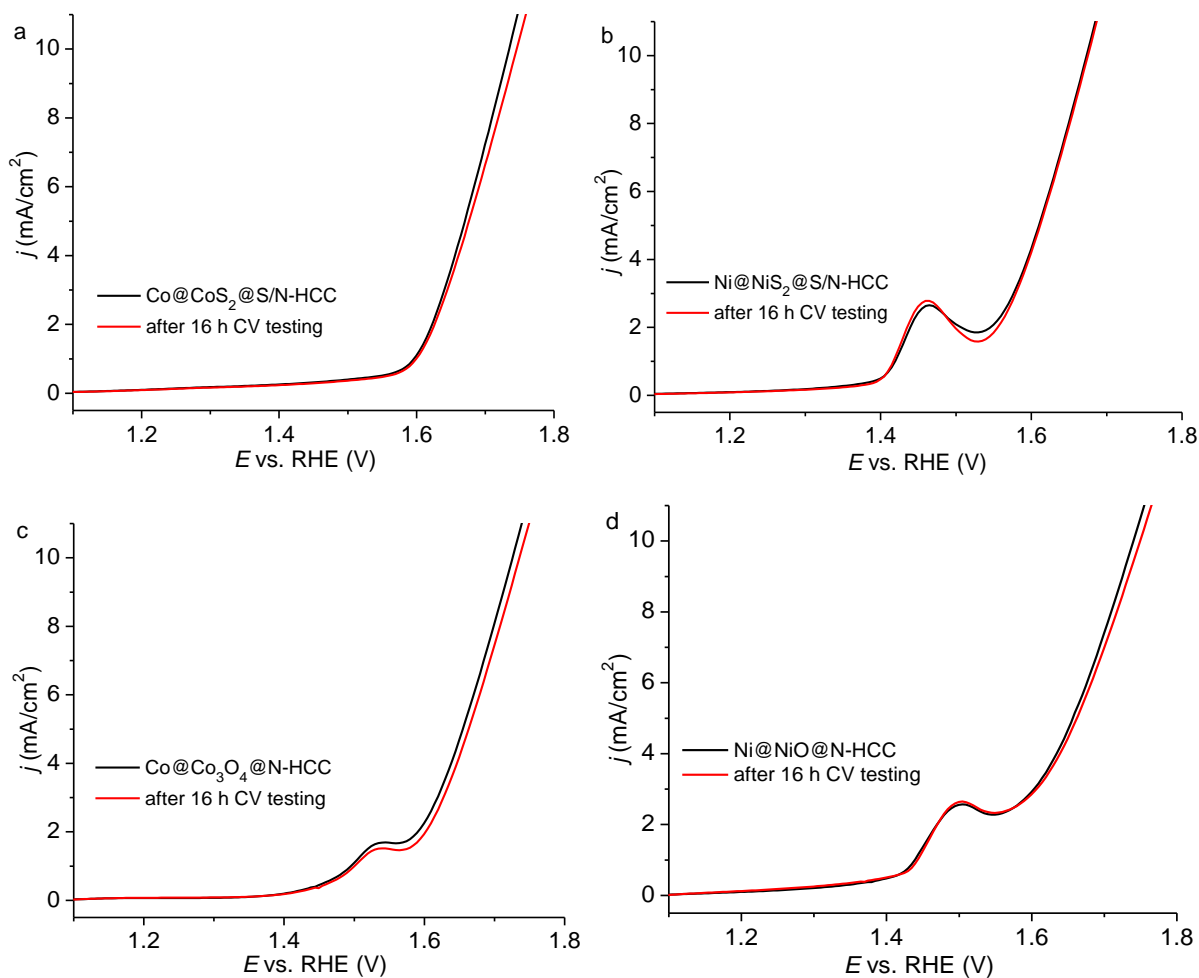
Fig. S38 Polarization curves of as synthesized samples before and after 16 h CV testing with a san rate of

50 mV/s in a 0.1 M KOH solution Co@CoS$_2$@S/N–HCC (a); Ni@NiS$_2$@S/N–HCC (b); Co@Co$_3$O$_4$@N–HCC

(c); Ni@NiO@N–HCC (d). All potentials are given without iR correction
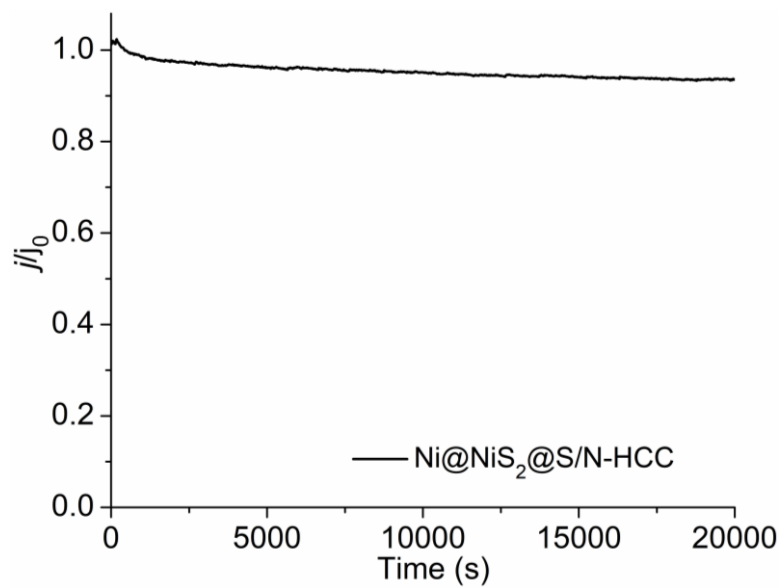
**Fig. S39** Chronoamperometry curve of Ni@NiS$_2$@S/N−HCC at 1.67 V vs. RHE in 0.1 M KOH.

Table S1 ORR activities of the as−synthesized and reported materials in alkaline solution (electrode rotating speed is 1600 rpm, in 0.1 M KOH solution)

catalysts	Loading mass (mg cm^{-2})	E_{onset} (V)	E_{half} (V)	$C_{density}$ (mA cm^{-2})	Ref.
Co@CoS$_2$@S/N−HCC	0.1	1.0	0.86	5.8 (at 0.6 V)	this work
Ni@NiS$_2$@S/N−HCC	0.1	0.92	0.81	4.6 (at 0.6 V)	this work
Co@Co$_3$O$_4$@N−HCC	0.1	0.96	0.84	5.7 (at 0.6 V)	this work
Ni@NiO@N−HCC	0.1	0.93	0.81	5.1 (at 0.6 V)	this work
Co@Co$_3$O$_4$@C−CM	0.1	0.93	0.81	~4.3 (at 0.6 V)	[2]
Fe−N/C−800	0.1	0.923	0.81	~ 6 (at 0.6 V)	[3]
Fe−N−CNT−OPC	0.4	~0.96		~ 6 (at 0.5 V)	[4]
Fe−N−CNFs	0.6	0.93		5.12 (at 0.26V)	[5]
Fe$_X$@NOMC	0.25	~0.9		~5.5 (at 0.5 V)	[6]
Fe$_3$C/NG−800	0.4	1.03	0.86	~ 6 (at 0.6 V)	[7]
PCN−FeCo/C	0.2	1.0	0.85	~ 5 (at 0.6 V)	[8]
PCNCo−20	0.1	0.92	0.84	~ 6 (at 0.6 V)	[9]
Fe−N−Carbon	0.0796	0.98		4.81 (at 0.45 V)	[10]
Amaranthus derived carbon	n/a	1.135		4.38 (at 0.265 V)	[11]
Co−TA−800	0.3	0.95		4.2 at 0.60 V	[12]
FP−Fe−TA−N−850	0.3	0.98		5.0 (at 0.60 V)	[13]
Co$_3$O$_4$/NPGC	0.2	0.97		5.84 (at 0.60 V)	[14]
NCNTFs	0.2	1.0		~ 5 (at 0.60 V)	[15]
N−Fe−CNT	0.2		0.87		[16]
Co$_3$O$_4$/N−G	0.1	0.88	~0.83		[17]

Fe,N,S–codoped carbon	0.1		~0.81	[18]
S–Doped G			~0.73	[19]
B,N–doped CNTs			~0.75	[20]
N,S–codoped carbon	0.28		~0.82	[21]
CNT–G	0.485		~0.87	[22]
N–doped G	0.051		~0.73	[23]
SHG	0.2	1.01	0.87	[24]
g–C$_3$N$_4$/carbon	0.085		~0.7	[25]
Fe$_3$C/C–800	0.6	1.05	0.83	[26]
NPC–Co45		0.9	0.79	[27]
Co@Co$_3$O$_4$/NC–1	0.21			[28]

Table S2 ORR and OER activities of the as–synthesized and reported bifunctional catalysts in alkaline solution (0.1 M KOH solution)

catalysts	Loading mass (mg cm^{-2})	ORR E$_{half}$ (V)	OER E$_{OER}$ η@10 mA cm^{-2} (V)	ΔE (E$_{OER}$–E$_{ORR}$) (V)	Ref.
Co@CoS$_2$@S/N–HCC	0.1	0.86	1.73	0.87	this work
Ni@NiS$_2$@S/N–HCC	0.1	0.81	1.67	0.86	this work
Co@Co$_3$O$_4$@N–HCC	0.1	0.84	1.72	0.88	this work
Ni@NiO@N–HCC	0.1	0.81	1.74	0.93	this work
Co–TA–800	0.3	0.81 (at 3 mA cm^{-2})	1.69	0.88	[12]

Co@Co$_3$O$_4$/NC$-$1	0.21	0.8 (at 3 mA cm^{-2})	1.65	0.85	[28]
NGM	0.25	0.77	1.67	0.9	[29]
GM	0.25	0.68	1.64	0.96	[29]
N$-$carbon nanotube frameworks	0.2	0.87	1.60	0.73	[15]
ZIF$-$derived carbon	0.36		1.75	~ 6 (at 0.6 V)	[30]
N/Co$-$doped MOF derived carbon/NRGO	0.36		1.66	~ 5 (at 0.6 V)	[30]
PCN$-$CFP	~0.2	0.67	1.63	0.96	[31]
Pt/C		0.96@1mA cm^{-2}	1.9	0.94	[32]
Ir/C	n/a	0.69	1.61	0.92	[33]

REFERENCES

1. S. R. Venna, J. B. Jasinski, M. A. Carreon, *J. Am. Chem. Soc.,* 2010, **132**, 18030–18033.

2. W. Xia, R. Q. Zou, L. An, D. G. Xia, S. J. Guo, *Energy Environ. Sci.*, 2015, **8**, 568–576.

3. L. Lin, Q. Zhu, A. W. Xu, *J. Am. Chem. Soc*., 2014, **136**, 11027–11033.

4. L. Liang, R. F. Zhou, X. M. Chen, Y. H. Tang, S. Z. Qiao, *Adv. Mater.*, 2014, **26**, 6074–6079.

5. Z. Y. Wu, X. X. Xu, B. C. Hu, H. W. Liang, Y. Lin, LF. Chen, S. H. Yu, *Angew. Chem. Int. Ed*., 2015, **54**, 8179–8183.

6. Z. Li, G. Li, L. Jiang, J. Li, G. Sun, C. Xia, F. Li, *Angew. Chem. Int. Ed.*, 2015, **54**, 1494–1498.

7. M.L. Xiao, J. B. Zhu, L. G. Feng, C. P. Liu, W. Xing, *Adv. Mater.*, 2015, **27**, 2521–2527.

8. Q. P. Lin, X. H. Bu, A. G. Kong, C. Y. Mao, F. Bu, P. Y. Feng, *Adv. Mater.,* 2015, **27**, 3431–3436.

9. Y. Z. Chen, C. M. Wang, Z. Y. Wu, Y. J. Xiong, Q. Xu, S. H. Yu, H. L. Jiang, *Adv. Mater*. 2015, **27**, 5010–5016.

10. W. H. Niu, L. G. Li, X. J. Liu, N. Wang, J. Liu, W. J. Zhou, Z. H. Tang, S. W. Chen, *J. Am. Chem. Soc*., 2015, **137**, 5555–5562.

11. S. Y. Gao, K. R. Geng, H. Y. Liu, X. J. Wei, M. Zhang, P. Wang, J. J. Wang, *Energy Environ. Sci*., 2015, **8**, 221–229.

12. J. Wei, Y. Liang, Y. X. Hu, B. Kong, J. Zhang, Q. F. Gu, Y. P. Tong, X. B. Wang, S. P. Jiang, H. T. Wang, *Angew. Chem. Int. Ed.*, 2016, **55**, 12470–12474.

13. J. Wei, Y. Liang, Y. Hu, B. Kong, G. P. Simon, J. Zhang, S. P. Jiang, H. Wang, *Angew. Chem. Int. Ed*., 2016, **55**, 1355–1359.

14. G. Li, X. Wang, J. Fu, J. Li, M. G. Park, Y. Zhang, G. Lui, Z. Chen, *Angew. Chem. Int. Ed.*, 2016, **55**, 4977–4982.

15. B. Y. Xia, Y. Yan, N. Li, H. B. Wu, X. W. Lou, X. Wang, *Nat. Energy,* 2016, **1**, 15006–15013.

16. H. T. Chung, J. H. Won, P. Zelenay, *Nat. Comm.*, 2013, **4**, 1922–1926.

17. Y. Y. Liang, Y. G. Li, H. L. Wang, J. G. Zhou, J. Wang, T. Regier, H. J. Dai, *Nat. Mater.*, 2011, **10**, 780–786.

18. Y. Q. Chang, F. Hong, C. X. He, Q. L. Zhang, J. H. Liu, *Adv. Mater.*, 2013, **25**, 4794–4799.

19. Z. Yang, Z. Yao, G. F. Li, G. Y. Fang, H. G. Nie, Z. Liu, X. M. Zhou, X. A. Chen, S. M. Huang, *ACS Nano*, 2011, **6**, 205–211.

20. S. Y. Wang, E. Iyyamperumal, A. Roy, Y. H. Xue, D. S. Yu, L. M. Dai, A*ngew. Chem. Int. Ed.*, 2011, **50**, 11756–11760.

21. X. F. Liu, M. Antonietti, *Adv. Mater.*, 2013, **25**, 6284–6290.

22. Y. G. Li, W. Zhou, H. L. Wang, L. M. Xie, Y. Y. Liang, F. Wei, J. C. Idrobo, S. J. Pennycook, H. J. Dai, *Nat. Nanotech.* 2012, **7**, 394–400.

23. K. Parvez, S. Yang Y., Hernandez, A. Winter, A. Turchanin, X. Feng, K. Müllen, *ACS Nano*, 2012, **6**, 9541–9550.

24. C. G. Hu, L. M. Dai, *Adv. Mater.*, 2017, **29**, 1604942–1604950.

25. J. Liang, Y. Zheng, J. Chen, J. Liu, D. Hulicova–Jurcakova, M. Jaroniec, S. Z. Qiao, *Angew. Chem. Int. Ed.*, 2012, **51**, 3892–3896.

26. Y. Hu, J. O. Jensen, W. Zhang, L. N. Cleemann, W. Xing, N.J. Bjerrum, Q. Li, *Angew. Chem. Int. Ed.,* 2014, **53**, 3675–3679.

27. Z. Y. Liu, G. X. Zhang, Z. Y. Lu, X. Y. Jin, Z. Chang, X. M. Sun, *Nano Res.*, 2013, **6**, 293–297.

28. A. Aijaz, J. Masa, C. Rösler, W. Xia, P. Weide, M. Alexander, J. R. Botz, R. Fischer, W. Schuhmann, M. Muhler, *Angew. Chem. Int. Ed.*, 2016, **55**, 4087–4091.

29. C. Tang, H. F. Wang, X. Chen, B.-Q. Li, T. Z. Hou, B. S. Zhang, Q. Zhang, M. M. Titirici, F. Wei, *Adv. Mater.*, 2016, **28**, 6845–6851.

30. Y. Hou, Z. H. Wen, S. M. Cui, S. Q. Ci, S. Mao, J. H. Chen, *Adv. Funct. Mater.* 2015, **25**, 872–882.

31. T. Y. Ma, J. R. Ran, S. Dai, M. Jaroniec, S. Z. Qiao, *Angew. Chem. Int. Ed.*, 2015, **54**, 4646–4650.

32. J. Masa, W. Xia, I. Sinev, A. Q Zhao, A. Y. Sun, S. Grützke, P. Weide, M. Muhler, W. Schuhmann, *Angew. Chem. Int. Ed.*, 2014, **53**, 8508–8512.

33. Y. Gorlin, T. A Jaramillo, *J. Am. Chem. Soc.*, 2010, **132**, 13612–13614.